Sclerostin Antibody-Loaded Dense Collagen Hydrogels Promote Critical-Size Bone Defect Repair

Ludovic Sicard, Sophie Maillard, Daline Mbita Akoa, Coralie Torrens, Anne-Margaux Collignon, Thibaud Coradin, Catherine Chaussain

Title

Sclerostin antibody-loaded dense collagen hydrogels promote critical-size bone defect repair.

Authors

Ludovic Sicard[a, b], Sophie Maillard[a], Daline Mbita Akoa[c], Coralie Torrens[a], Anne-Margaux Collignon[a,b], Thibaud Coradin[c*], Catherine Chaussain[a,b,d,*]

Affiliations

[a]Université Paris Cité, Institut des Maladies Musculo-Squelettiques, Orofacial Pathologies, Imaging and Biotherapies Laboratory URP2496 and FHU-DDS-Net, Dental School, and Plateforme d'Imagerie du Vivant (PIV), 92120 Montrouge, France.

[b]AP-HP, Dental Medicine Departments, Bretonneau and Louis Mourier Hospitals, GHN-Université Paris Cité, 75018 Paris, France.

[c]Sorbonne Université, CNRS, Laboratoire de Chimie de la Matière Condensée de Paris (LCMCP), UMR 7574, 4 place Jussieu, 75005 Paris, France.

[d]AP-HP, Reference Center for Rare Disorders of the Calcium and Phosphate Metabolism, Dental Medicine Department, Bretonneau Hospital, GHN-Université Paris Cité, 75018 Paris, France.

*Corresponding authors: Catherine Chaussain catherine.chaussain@u-paris.fr; Thibaud Coradin: thibaud.coradin@sorbonne-universite.fr

Abstract

The management of extensive bone loss remains a clinical challenge. Numerous studies are underway to develop a combination of biomaterials, biomolecules and stem cells to address this challenge. In particular, the systemic administration of antibodies against sclerostin, a regulator of bone formation, was recently shown to enhance the bone repair efficiency of dense collagen hydrogels hosting murine dental pulp stem cells (mDPSCs). The aim of the present study was to assess whether these antibodies, encapsulated and released from dense collagen hydrogels (DCHs), could promote craniofacial bone repair by local inhibition of sclerostin.

In vitro studies showed that antibody loading modified neither the hydrogel structure nor the viability of seeded mDPSCs. When implanted in a mouse calvaria critical-size bone defect, antibody-loaded DCHs showed repair capabilities similar to acellular unloaded DCHs combined with antibody injections. Importantly, the addition of mDPSCs provided no further benefit.

Altogether, the local delivery of anti-sclerostin antibodies from acellular dense collagen scaffolds is highly effective for bone repair. The drastic reduction in the required amount of antibody compared to systemic injection should reduce the cost of the procedure, making the here-proposed strategy a promising therapeutic approach for large bone defects repair.

Keywords: Bone tissue engineering; Monoclonal antibody therapy; Sclerostin; Collagen hydrogels; Dental pulp stem cells.

1. Introduction

Over the last 30 years, bone tissue engineering strategies have continuously improved the design of biomaterials with enhanced ability to promote osteogenesis through the combination of scaffolds, stem cells and biomolecules acting synergistically[1–5]. Scaffolds aim to mimic and delimit a biological microenvironment to allow cell migration and proliferation[6,7]. They can be prepared from a wide range of materials, which can be inert, bioactive or biological [8]. Their structure, mechanical stability and degradation kinetics can be varied to a large extent [9]. However, when implanted, scaffolds are susceptible to infection, especially because their limited vascularization can impede immune cells migration to the contaminated site [10,11]. To promote biological response, scaffolds can be seeded with stem cells[12]. Adult stem cells, including mesenchymal stem cells (MSCs), are preferred due to their safe profile compared to embryonic and induced pluripotent stem cells[13]. Adequately primed, they promote direct target tissue formation or indirect formation by secreting bioactive molecules[14,15]. Autologous MSCs are the best candidates to avoid any immune response[16]. However, the number of available cells is limited by the process time, mainly restricting their use to planned medical procedures[17]. Active molecules, such as antibiotics, growth factors or antibodies, can also be added to the scaffold, targeting either host cells, seeded cells or both[18–20]. Compared to systemic administration (e.g. intravenous dispensation), local delivery via a scaffold dispenses the medication close to the target site, reducing the total dose required and thus mitigating systemic adverse effects[21,22]. The two associated primary challenges are to maintain the bioactivity of the molecules during the scaffold loading step, especially in the case of antibodies[23], and to adjust the release kinetics *in vivo*.

To restore bone defects, especially critical-size ones, using dense collagen hydrogels (DCH) as scaffolds is a promising approach[15,24]. They are soft, biocompatible, biodegradable, and with a fibrillar density that can be similar to that of the native bone matrix[25–27]. They can be seeded with MSCs to promote bone repair by accelerating osteogenic differentiation[28]. Dental Pulp Stem Cells (DPSCs) are a type of MSCs commonly used that can be differentiated into multiple lineages including bone-forming cells[29]. Adequately primed and seeded into DCHs, they enhance bone repair *in vivo*[15,24]. DPSCs are eligible candidates for craniofacial bone

therapy as they are derived from the same embryological origin as the skull bones, the neural crest[30].

Bone cell activity is under the dependence of two main signaling pathways: (a) the SMAD(x) pathway, with ligands such as BMP and TGF-β, and (b) the Wnt (wingless-related integration-site)/β-catenin pathway involving proteins such sclerostin, an inhibitor of this pathway[31,32]. Sclerostin is the protein encoded by the *SOST* gene, whose loss-of-function mutations lead in uncontrolled bone apposition (hyperostosis corticalis generalisata disease)[33,34]. Monoclonal antibodies against sclerostin (Scl-Ab) were developed to increase bone formation and are currently used to improve bone quality in osteoporosis and osteogenesis imperfecta, a rare bone fragility disorder[35,36]. Repeated systemic injection of Scl-Ab has already proven a promising approach to favor bone healing[37]. Monthly delivery of Sclerostin single-chain antibody fragments loaded in poly(lactic-co-glycolic acid) (PLGA) microspheres was shown to promote long-bone fracture healing in ovariectomized rats[38]. In a step further, we have recently shown that implementing a DCH scaffold, with or without mDPSCs, combined with weekly intravenous (IV) injection of Scl-Ab over two months enhanced bone formation in a calvarial critical bone defect[39]. In addition, implementing a DCH seeded with *Sost* knock-out (KO) mDPSCs in a wild-type (WT) mouse calvaria critical-size bone defect similarly promoted bone formation, suggesting that the local inhibition of sclerostin may be sufficient to improve bone healing[39]. Taken together, these data suggest that the direct loading of the Scl-Ab into the DCH could reproduce this local inhibition within the bone defect, reducing the global dose delivered, thus limiting potential side effects such as mild reaction at the injection site, and reducing the treatment cost[35].

Current research on antibody-loaded hydrogels focuses on PLGA, chitosan, alginate, collagen, or hyaluronic acid-based scaffolds[40]. Injectable antibody-loaded hydrogels were developed for possible use in ocular drug delivery, cancer or stroke treatments[41]. Whereas several antibody-releasing materials have been recently developed for subcutaneous implantation[42,43], *in situ* placement of hydrogels loaded with full antibody for bone repair has not been described yet. Therefore, in the present study, we aimed at assessing whether the Scl-Ab loading of DCH scaffolds could improve the efficacy of bone regeneration in craniofacial defects. To this end, we evaluated the antibody-loading capacity of DCH and the survival of seeded mDPSCs at the selected doses. Critical craniofacial bone defects created in adult mice

were filled with Scl-Ab-loaded DCH, either cellularized with mDPSCs or acellular, and bone formation was monitored within the defects. Ultimately, the best condition was compared to the standard condition, e.g. mice treated with DCH combined with Scl-Ab IV injections.

2. Materials and Methods

2.1. Ethical approval and animal management

All experiments in this study were conformed to ARRIVE (Animal Research: Reporting of in vivo Experiments) guidelines and were approved by the Animal Care Committee of the Université Paris-Cité (APAFIS agreement # 24,297 N°2,019,022,017,023,656). Animals were maintained according to the guidelines for ethical conduct developed by the European Communities Council Directive (animal breeding agreement C92–049–01). All efforts were made to minimize their pain or discomfort. Seventy-six ten-week-old male mice with a C57BL/6 J genetic background were used for this study and were housed in stable conditions (22 ± 2 °C) with a 12 h dark/light cycle and with ad libitum access to water and food.

2.2. Isolation and culture of dental pulp stem cells (mDPSCs)

Multi-colony-derived mouse dental pulp stem cells (mDPSCs) were obtained from the molars of three-day postnatal (PN3) littermate WT mice using a protocol adapted from Gronthos et al.[29]. Briefly, murine molar gems were collected under sterile conditions and incubated at 4 °C for 45 min in phosphate-buffered saline (PBS) containing 100 $U.mL^{-1}$ penicillin/streptomycin (Gibco, Hampton, USA) and 250 $\mu g.mL^{-1}$ fungizone (Gibco), and then in PBS containing 3 mg.mL-^{1} type I collagenase (Worthington Biochem, Freehold, NJ, USA) and 2 $U.mL^{-1}$ dispase I (Roche, Mannheim, Germany) in a shaking incubator (at 37 °C) for one hour. The isolated cells were then plated on 0.1 % gelatin-coated dishes in Minimum Essential Media-alpha (Gibco) supplemented with 20 % v/v fetal bovine serum (FBS) (Gibco), 100 $U.mL^{-1}$ Penicillin/streptomycin (Gibco), 2.5 ng. mL^{-1} FGF-2 (PeproTech, Neuilly Sur Seine France), 10 ng mL^{-1} BMP-2 (PeproTech) and maintained at 37 °C under 5% CO_2 atmosphere. The medium was changed after two days, then three times a week. The required cell number for *in vivo* experiments was reached after two to three passages.

2.3. Dense Collagen Hydrogel (DCH) preparation

Plastically compressed collagen gels were used as three-dimensional scaffolds and prepared as previously described[39,44]. Briefly, 1.8 mL of a sterile rat-tail tendon type I collagen solution at a protein concentration of 3.5 $mg.mL^{-1}$ in 0.1% acetic acid, obtained as previously described,[45] was mixed with 0.4 mL of 10X Dulbecco's Modified Eagle Medium (DMEM) and 0.4 mL 10X $NaHCO_3$. Neutralization was achieved by drop-wise addition of 0.1 N NaOH until pH = 7.4. After neutralization, the mixture was completed to 4 mL with Minimum Essential Media-alpha (Gibco), with or without mDPSCs at a seeding density of $2x10^6$ cells per mL, with or without Scl-Ab (Setrusumab, BPS804; kind gift from Mereo Biopharma (London, UK)) and was ice-cold mixed. The mixture was then dispensed into a four-well plate. After gelling (30 min at 37 °C), highly hydrated hydrogels were placed on a stack of blotting paper, nylon, and stainless steel meshes as described in Coyac et al[44]. Dense collagen hydrogels (DCH) were produced by the application of an unconfined compressive stress of 2 kPa for five min to remove excess casting fluid.

For *in vivo* experiments, hydrogels were prepared with or without antibodies, and with or without cells. Scl-Ab loaded DCHs were prepared with two different concentrations of antibody in the initial solution, 0.2 $mg.mL^{-1}$ and 2 $mg.mL^{-1}$, hereafter-termed low dose (Ld) and high dose (Hd), respectively. Cell seeding density was always $2x10^6$ cells per mL. After compression, DCHs were circularly cut (four mm in diameter, in aqueous medium) and kept up to 24 h at 37 °C under 5% CO_2 in serum-free medium before implantation. DCHs were kept in a serum complemented with Scl-Ab at the same concentration as the initial solution.

The antibody was reconstituted with water for injection (WFI). For injection, the stock solution was diluted in saline solution[39].

2.4. Characterization of the DCH

To assess the volume of the DCH before and after compression, 20 µL per DCH of a barium sulphate suspension (0.1 $g.mL^{-1}$, Micropaque, GUERBET lab) were added to obtain radio dense samples (n=8). DCHs were imaged before and after compression using an X-ray micro-CT

device (see below). Using DICOM image stacks, the DCH were segmented, and their volumes assessed using AVIZO software (v2019.1, ThermoFisher Scientific).

Gels were imaged before and after compression by Scanning Electron Microscopy (SEM). Gels were fixed with 4% paraformaldehyde (PFA) in phosphate-buffered saline (PBS). After rinsing with a 0.1 M cacodylate/0.6 M sucrose buffer, they were dehydrated in water:ethanol solutions of increasing alcohol content and dried using supercritical CO_2. Samples were sputter-coated with a gold layer (15 nm) and imaged using a Hitachi S-3400 N SEM microscope operating at 10 kV.

2.5. Assessment of the Scl-Ab distribution, loading and release kinetics

To evaluate the distribution of the antibody within the hydrogel, 100µg of Scl-Ab was labelled using the SiteCLick Antibody Labelling Kit (S10467) from Invitrogen. Briefly, it consists of a three-step workflow: modification of the carbohydrate domain of the antibody, azide attachment to the antibody and conjugation with a DIBO-modified R-phycoerythrin. The labelled Scl-Ab was added to unlabelled Scl-Ab to produce a Hd DCH (n=1), resulting in a hydrogel containing 5% labelled Scl-Ab (100µg labelled /2mg total Scl-Ab) prior to compression. After plastic compression, the hydrogel was imaged by confocal microscopy.

To assess Scl-Ab loading of the hydrogels after compression, DCH were digested in a solution of 225 µL of PBS and 25 µL of type I collagenase (290 $U.mg^{-1}$). An Enzyme Linked Immuno-Sorbent Assay (ELISA) (ABCAM ab195215 – IgG Human SimpleStep ELISA Kit) was then performed according to the recommendations of the manufacturer. Each measure was done in duplicate with each condition in triplicate. A solution of collagenase alone and one of collagenase with a known concentration of antibody were used as controls. The results were adjusted with the OD of the collagenase solution. The concentration of the collagenase/antibody solution was in the range of the initial solution (3.5 $mg.mL^{-1}$). Plates were read on an Infinite 200 M-Plex plate reader (Tecan).

To study Scl-Ab release kinetics from the hydrogels, they were placed immediately after compression in 0.5 mL of PBS at 37°C. After 3, 6, 9, 24, 31, 57, 82 and 101 hours, 0.15 mL of solution was removed and replaced by 0.15 mL of PBS. The antibody concentration in each

sample was measured by ELISA. To assess the possible effect of cellularization on Scl-Ab release, similar experiments were performed using mDPSCs-seeded hydrogels.

2.6. In vitro assessment of cell viability

Cell viability and distribution within the dense collagen scaffolds were assessed using the Live/Dead® cell viability-cytotoxicity assay (Invitrogen, Carlsbad, CA, USA) at 24 hours with a confocal laser scanning microscope (IXplore Spinning 522 Roussy), and using Alamar Blue assay (Invitrogen, Carlsbad, CA, USA) at days 1, 7, 14, 21 and 28. For the Live/Dead assay, image acquisition was performed in IMAG'IC Facility, member of the National Infrastructure France BioImaging (ANR-10-INBS-04). Images from the Live/Dead assay were analyzed with Fiji[46]. Alamar blue assay was performed and analyzed following the manufacturer instructions.

2.7. Surgical implantation

Mice were anesthetized (100 mg/kg b.w. of ketamine and 10 mg/kg b.w. of xylazine hydrochloride, both from Centravet Alfort, Maisons-Alfort, France). In each individual, scalp skin was incised to visualize the periostium. A 3.5 mm diameter calvaria critical-sized defect[47] was created on each side of the parietal bone using a mucosa punch (Helmut Zepf 08.920.13) attached to a slow speed hand piece operating at 3000 rpm, under constant irrigation with sterile saline solution (NSK – Viva Ace). Special care was taken for the sagittal suture preservation, and minimal invasion of the dura mater. After gently removing the circular bone plug, DCH were implanted in each of the two bone defects (same DCH condition in the two defects)[47]. Two control groups were performed: defect left empty and sham, which consisted in skin opening without bone removal. Each animal was randomly allocated per cage and per group. Wound closure was achieved by a suturing (skin) using absorbable sutures (Vicryl Rapid 4.0, Ethicon, Johnson & Johnson). Immediate post-operative care included analgesia with buprenorphine (0.02 mg/kg b.w.). After surgery, mice were housed by 4 under constant conditions. Wound healing progress, material exposure or other complications were monitored daily. Body weights were monitored regularly to ensure proper feeding before and after surgery. Mice were euthanized at the end of the eight-week intervention period, i.e., at the age of 18 weeks.

2.8. Micro-X-ray computed tomography (Micro-CT) examination of samples.

For bone regeneration exploration, mice were anesthetized (isoflurane, induction at 2–2.5 % under airflow of 0.8–1.5 $L.min^{-1}$; 11.5 % under 400–800 $mL.min^{-1}$ thereafter) and were imaged using an X-ray micro-CT device (Quantum FX Caliper, Life Sciences, Perkin Elmer, Waltham, MA) hosted by the PIV Platform, URP2496, Montrouge, France. The X-ray source was set at 90 kV for the voltage and 160 µA for the intensity. Tri-dimensional images were acquired with an isotropic voxel size of 20 µm. Tri-dimensional rendering was subsequently extracted from DICOM image stacks using CTvox rendering software (v3.3.1, Bruker microCT). Before quantification, image stacks were reoriented using DataViewer (Skyscan, release 1.5.6.2, Kontich, Belgium) to the center of the defect. Then, quantification of the regenerated bone was performed with a cylindrical shape volume of interest of 3.5 mm of diameter and 1 mm height, using CT-Analyzer software (Skyscan, release 1.20.8.0, Kontich, Belgium). An adaptative thresholding was performed with a radius of two, between 364.34 and 560.82 $mgHA.cm^{-3}$ (HA: Hydroxyapatite). To reduce background, open/close morphological operations (radius = 1) were performed on the segmented bone. Bone volume fraction BV/TV (BV: Bone volume and TV: Total volume) (%), total porosity (%) and Bone Mineral Density (BMD, $mgHA.cm^{-3}$) were used to quantify and characterized newly repaired bone. Since the regenerated bone is mainly a compact bone, trabecular thickness Tb.Th (mm), trabecular number Tb.N (one per mm) and trabecular separation Tb.Sp (mm) were not described as they apply to trabecular bone only[48].

2.9. Histology, histomorphometry

At two months, mice were sacrificed for histological analysis. Half heads were fixed for 36 hours in 4% paraformaldehyde at 4°C under constant agitation. After preservation only of the calvaria and adjoining brain, the hard tissue demineralization was obtained using a microwave (KOS, Milestone, Shelton, CT, USA) in a 4.13% EDTA (pH 7.4) solution changed every 2 days for 2 weeks. The samples were subsequently embedded in Diawax (Diapath), serial sagittal sections of 5 µm were cut with a microtome. Deparaffinized sections were stained with Masson's trichrome.

The remaining two-months non-decalcified samples were fixed in 70 % vol/vol ethanol for 24 h at 4°C, dehydrated in graded ethanol solutions and embedded at −20 °C in methyl-methacrylate resin (Merck & Co., Whitehouse Station, NY). Five-µm thick deplastified calvaria bone sample sections were sequentially cleared in an alcohol gradient and in water then stained with von Kossa staining or processed for alkaline phosphatase (ALP) enzyme-histochemistry and for tartrate-resistant acid phosphatase (TRAP) revelation[49]. Von Kossa staining was used to visualize mineralized bone by using silver nitrate (Sigma). TRAP was detected by using Naphtol ASTR phosphate (Sigma) and Fast Red TR Salt (Sigma) to reveal osteoclasts; non osteoclastic acid phosphatase was inhibited by adding 100 mM L(+)-tartric acid (Sigma, St Louis, MO) to the substrate solution. ALP was detected by using Naphtol ASTR Phosphate, NN-Diméthylformamide, Fast Blue RR Salt and $MgCl_2$.

Image acquisition was performed using a Lamina multilabel slide scanner (Perkin Elmer) hosted by the HistIM platform at the Institut Cochin, Paris. Slide visualization was performed with CaseViewer, 3DHISTECH's advanced slide viewing software.

2.10. Second Harmonic Generation microscopy

Second harmonic generation microscopy offers the possibility to image collagen without staining, as previously described[50]. The calvaria imaging was performed using a multiphoton inverted stand Leica SP8 DIVE microscope (Leica Microsystems GmbH, Wetzlar, Germany) located at the IMAG'IC core-facility at the Institut Cochin, Paris. The laser source used for generating second harmonic (SHG) and two photon-excited fluorescence (TPEF) signals was a Ti:Sapphire Chameleon Ultra (Coherent, Saclay, France) tuned at 810 nm. The laser beam was circularly polarized, and excitation and collection of SHG and TPEF signals were performed using a Leica Microsystems HCX IRAPO 25 × /0.95 W objective. Signals were detected in epi-collection using 405/15 nm and 525/50 bandpass filters, respectively, by NDD PMT detectors (Leica Microsystems) with a constant voltage supply. LAS X software (Leica, Germany) was used for laser scanning control and image acquisition.

2.11. Confocal microscopy

Imaging was performed using a Leica Microsystem SP8X confocal microscope (Leica Microsystems GmbH, Wetzlar, Germany) located at the IMAG'IC core-facility at the Institut Cochin, Paris, with a x20 objective (0.75NA, dry), an image size of 512x512 pixels, a Z step of 2µm, an excitation wavelength of 565nm with a 5% gain and a detection range between 578 and 610nm. Z acquisition was performed over 500µm. LAS software (Leica, Germany) was used for laser scanning control and image acquisition.

2.12. Statistical analyses

Numerical variables are expressed as the mean ± standard deviation (SD). The statistical analyses were performed using Prism software version 9.0.2 (GraphPad software, La Jolla, CA). The normality of the distribution was tested with the D'Agostino Pearson omnibus normality test and the homogeneity of variance was tested with the Fisher F test. For multiple comparisons, when data was following a normal distribution with variances significantly different between groups, a Brown-Forsythe and Welch ANOVA parametric test allowing the comparison between more than two independent samples was performed. If the distribution was not following a normal distribution, a Kruskal-Wallis test was performed. For in vivo experiments, as two defects were performed for each animal, the bone defect was considered as the statistical unit. Differences were considered significant at $P < 0.05$. A Šídák's multiple comparisons correction was performed for multiple comparisons.

3. Results

3.1. Scl-Ab loading and release from DCH

Collagen hydrogels prepared from 1 mL solution at 1.6 $mg.mL^{-1}$ of collagen were densified by plastic compression[28,44]. Before compression, the hydrogels (n=4) had a mean base diameter of 15.4 ± 0.6 mm and mean thickness of 2.5 ± 0.2 mm. After compression, there was no significant change in the gel diameter (16.0 ± 0.5 mm). The thickness was significantly different with a *ca*. 11-fold reduction (0.23 ± 0.02 mm) (Fig. 1A, S1A, S1B). The mean volume of the hydrogels before plastic compression was 410 ± 40 mm^3 compared to the initial volume of 1000 mm^3 before gelling. The mean volume of the DCH (after compression) was 60 ± 20

mm^3 (Fig. 1B). This corresponds to a final collagen concentration of 23 mg.mL^{-1} in the DCH. SEM imaging showed that the uncompressed hydrogel consisted in a highly porous fibrillar network. After compression, the porosity decreased without modification of the fiber diameter (50 ± 10 nm) (Fig. 1C).

Confocal imaging showed a homogeneous spatial distribution of labelled Scl-Ab within the Hd DCH, accounting for 5% of the image area (5% in the initial solution), with the presence of focal dots and aggregates. (Fig. 1D). In sharp contrast, no signal was found in the absence of Scl-Ab (data not shown).

Increasing amounts of Scl-Ab were introduced in the collagen solution after neutralization. As seen in Fig.1D, the amount of loaded antibody in the final DCH increased linearly with initial antibody amount until reaching a plateau for an initial antibody amount of *ca*. 1 mg leading to *ca*. 0.2 mg of Scl-Ab within the DCH (Fig. 1E). Based on these results, two concentrations were selected for the rest of the study: (a) one before the plateau, at 0.2 mg.mL^{-1} in the initial solution, corresponding to 0.008 mg in the DCH (low dose, Ld) and (b) one at the beginning of the plateau, at 2 mg.mL^{-1} in the initial solution, corresponding to 0.2 mg in the DCH (high dose, Hd). Concentration exceeding 2 mg.mL^{-1} (Hd) in the initial solution were considered to create a DCH with an unpredictable final Scl-Ab content as suggested by the large standard deviation of the measurements.

Regarding the release kinetics of the antibody from the DCHs in a PBS solution at 37°C, a burst occurred in the first 9 hours to reach a plateau asymptotic to the initial loading, 0.008 mg and 0.2 mg for (a) and (b), respectively. Sampling was stopped at 24 hours for the Ld hydrogel because the plateau was reached as soon as the 9th hour, at least in the sensitivity range of the ELISA (Fig. 1F).

3.2. Scl-Ab loaded DCH implantation potentiates the outcomes of bone reparation strategy.

A first *in vivo* experiment was designed to test the efficacy of the two different Scl-Ab loadings, 0.2 mg.mL^{-1} (Ld) and 2 mg.mL^{-1} (Hd), within acellular DCH (Fig.2). Four-mm-DCH cut from the main DCH were implanted in mouse calvaria critical defects and bone formation was monitored for 2 months. Defects filled with acellular Scl-Ab-loaded DCHs were compared with

either empty defects or defects filled with unloaded acellular DCH (Fig. 2A). Micro-CT follow-up revealed an almost complete closure of the defects in mice treated with the Scl-Ab-loaded DCH at high dose at 60 days compared with the other conditions, getting closer to the sham (Fig. S2A). Quantitative analysis of bone formation showed that the BV/TV was significantly higher for the Hd DCH condition compared to (a) the Ld DCH, (b) the DCH alone condition (at 60 days: 11 ± 4 % vs (a) 9 ± 4 %, $p<0.05$, vs (b) 6 ± 3 %, $p<0.001$), and to the empty defect (at 30 days, 1 ± 1 %, $p<0.01$; at 60 days: 2 ± 1 %, $p<0.0001$) (Fig.2B). In contrast, no significant difference was found between Ld DCH and DCH alone, whereas at both time points, significantly increased bone formation was found in these two conditions compared to the empty defects. Similar results were found for bone mineral density (Fig. S7A) and for bone total porosity (Fig. 2C). Both micro-CT and histology analysis revealed that, in DCH groups, bone formation occurred mainly within the hydrogel, with sparse formation from the edges of the defects. In the Hd DCH, the resulting mineralized tissue was histologically comparable to a fully functional bone (Sham condition, Fig. S2B and C), with organized layers of collagen, bone marrow and red blood cells, osteocytes within the mineralized matrix and the gradual resorption of the DCH (Masson trichrome – Fig. 2D, SHG – Fig. 2E and S3), bordering osteoblasts (ALP activity) with an osteoid matrix, and osteoclasts (TRAP activity) (Fig. 2F). In the Ld DCH and DCH alone groups, the remaining DCH was surrounded by either newly formed bone or cell-rich connective tissue (Fig. S4).

3.3. Addition of mDPSCs within the Scl-Ab loaded DCH does not improve bone healing

We next assessed whether the addition of mDPSCs within the DCH, either with or without antibody, would improve bone formation within the defects, compared to the acellular Hd DCH (Fig. 3A). At both time points, a significant ($p<0.05$) and very significant ($p<0.01$) higher BV/TV was calculated in the acellular Hd DCH group compared to the three cellularized DCH conditions (Fig. 3B). Similar results were found for the total bone porosity (Fig 3C) and for bone mineral density (Fig. S7B). Histological analysis of the newly formed mineralized tissue at 60 days revealed a functional bone tissue in the four conditions (Fig. 3D and S5), with enhanced ALP and TRAP activities around the bone repaired area (Fig. 3E). However, in the mDPSCs-

seeded DCH conditions, non-mineralized DCH areas were colonized by elongated cells that followed the orientation of the collagen fibers, whereas, in the acellular condition, the non-mineralized DCH areas were deprived of cells (Fig. S6).

3.4. In vitro studies of SclAb – mDPSCs interactions within the DCH

As bone formation was not improved by the addition of mDPSCs, we assessed whether the addition of the antibody altered either cell survival or proliferation within the DCH by *in vitro* experiments. The live/dead assay at 24 hours presented no significant difference between mDPSCs-seeded DCH loaded with 0.2 and 2 $mg.mL^{-1}$ Scl-Ab (dead/live cell ratio of 0.05 ± 0.05, 0.4 ± 0.2 and 0.03 ± 0.02, respectively) with a homogeneous cell repartition for both dead and living cells (Fig. 4 A and B). Alamar Blue assay presented no significant difference at 0, 7, 14, 21 and 28 days, with a mean reduction rate between 30 and 40 % (Fig. 4C). We also hypothesized that the presence of mDPSCs may influence the release of the Scl-Ab from the DCH. However, no significant difference was found between the release kinetics profiles in Hd DCH and mDPSCs-Hd DCH (Fig. 4D).

3.5. Scl-Ab loaded DCH are as efficient as non-loaded DCH associated with Scl-Ab IV injection.

Ultimately, we sought to compare the effect of the local delivery of the antibody versus its systemic injection previously reported in Maillard et al[39]. For this purpose, bone formation within defects filled with acellular Hd DCH was compared to defects filled with acellular DCH combined with weekly injections of Scl-Ab. MicroCT analysis did not reveal significant difference between the two groups at both 30 and 60 days (BV/TV: 9 ± 4 % vs 10 ± 5 %, porosity 91 ± 4 % vs 90 ± 5 % respectively) (Fig. 5A, B and C). Same results were found for bone mineral density (Fig. S7C). Masson-trichrome staining showed a well-organized fully functional bony tissue (Fig. 5D), with a high osteoblast activity and osteoclast activity within the defects of both conditions (Fig. 5E) and parallel layers of collagen (SHG – Fig. 5F).

4. Discussion

Craniofacial lesions constitute a major public health issue as they are source of disabilities for patients and are very costly for health care systems[51]. There is a real need to develop innovative treatments to repair these lesions, especially in the growing field of tissue engineering[52,53]. Inhibiting Sclerostin is one of the therapeutic approaches currently developed for the treatment of unbalanced bone remodeling conditions[35]. Setrusumab (BPS804) is one of these anti-Sclerostin monoclonal antibodies. It has been granted Rare Pediatric Disease Designation by the FDA for osteogenis imperfecta treatment and was evaluated in a randomized phase 2a trial for this disease[36]. Another anti-sclerostin monoclonal antibody, Romozosumab, has already been FDA and EMA-approved to treat osteoporosis[54,55]. In the craniofacial bone context, we have previously reported that the systemic injection (IV) of Scl-Ab enhanced bone regeneration in critical size defects filled with dense collagen hydrogels, either acellular or cellularized with DPSC[39]. However, the weekly injection of monoclonal antibodies is expensive, may not be devoid of side effects, and seems difficult to promote for the treatment of a localized, even extensive, bone defect[35]. The aim of this study was therefore to assess whether the loading of Scl-Ab directly within dense collagen hydrogels, allowing for local delivery of these antibodies, could improve their bone regeneration capacity.

The design of hydrogels for the delivery of monoclonal antibodies has so far mainly considered these hydrogels as temporary supports for the delivery of the therapeutic molecule[23,40]. However, in the case of bone repair, these hydrogels must also play the role of a scaffold to fill the defect until new bone formation occurs. In particular, the possibility of using such scaffold for a dual function, *i.e*. antibody delivery and cellular hosting, in the context of tissue engineering has, to our knowledge, not been investigated so far.

In this context, type I collagen hydrogels appear particularly suitable as they are widely used for bone tissue engineering, most often in combination with bioactive particles, such as hydroxyapatite or bioglass[56–58]. However, collagen physical hydrogels are known to be poor drug delivery systems, mainly due to their high porosity and rapid biodegradation, at least at low density[59,60]. To address these issues, chemical modifications of the collagen fibers to enhance their affinity for the drug or even to achieve their covalent grafting, have been described[61,62]. Here, we hypothesized that using dense collagen networks exhibiting smaller pore size and slower biodegradation rates could improve their suitability as delivery systems.

However, only few methods leading to dense collagen hydrogels (DCH) are also compatible with cell encapsulation[25,63,64]. Among them, the plastic compression process has been shown to be effective hosts for a large number of cells[29,65–69]. In particular, it was shown to be compatible with the 3D immobilization of DPSC, that exhibiting mineralization capacity in vitro and bone repair activity in vivo[15,24,39,44]. However, the use of DCH for the delivery of antibodies or any other type of protein has not yet been described in the literature.

For the present project, as a first step, plastic-compressed collagen hydrogels appeared to be the most reproducible approach to deliver the monoclonal antibodies, while promoting bone formation[65,70,71]. Other materials have been used previously to design scaffolds for delivery of biomolecules and enhancement of bone repair, such as hyaluronic acid (HA), chitosan, alginate, or a combination of these[20,72]. Collagen-based hydrogels have been shown to promote cell invasion compared to hyaluronic acid-based hydrogel[73]. Chitosan hydrogels were shown to require fine-tuning of their degradation rate to promote bone repair[74], whereas DCH appeared to be less sensitive to initials conditions[65]. In the event of scaffold contamination during implantation, collagen naturally degrades, unlike non-absorbable materials such as alginate[75,76], which require surgical removal[77]. In the future, it will be important to test these materials associated or not with DCH in order to better control the delivery of the monoclonal antibodies.

Here, structural investigations of the hydrogels before and after compression have evidenced that the densification process leads to a decrease in the collagen network volume by a factor of *ca*. 10. At the same time, the amount of antibody within the collagen gel at saturation decreased by a similar factor. This suggests that the antibody did not interact significantly with the collagen fibers but rather remained located within the pores of the hydrogel. The spatial distribution of the antibodies supports this hypothesis, as they were not distributed along the collagen fibers, but rather in dots or clusters with a uniform repartition. Even though SEM images suggest a decrease in collagen network porosity after compression, observable mesh size remains above several hundred nanometers, i.e. much larger than the dimensions of antibodies (*ca*. 10 nm). As a result, the delivery process should occur by a simple diffusion process, explaining the observed burst effect.

The optimal response was obtained with the highest concentration of the antibody. In this condition, as well as in all other conditions where DCH was implanted, bone formation was

initiated within the hydrogel, from its border to its center. Whenever mineralization occurred within the DCH, the new tissue displayed all the characteristics of bone tissue including organized layers of collagen, osteoclast and osteoblast activity and robust well-distinguishable vascularization, albeit at a much higher level with antibody-loaded DCH.

Eventually, we have shown that there was no significant difference in bone reparation between the use of the antibody loaded DCH and the DCH alone with intravenous injection of the antibody. In the IV group, a total of 12 mg of antibody was used per mice (50mg/kg for a 30 mg mouse, once a week over 2 months) compared to 0.025 mg per mouse in the Scl-Ab loaded DCH group, delivered as a single dose. This very significant dose reduction should limit reported side effects[35,78,79]. Moreover, even if the encapsulation yield of the plastic compression is low (*ca*. 10 %), the required antibody amount remains significantly lower that for a systemic treatment, giving this method an economic advantage, especially to treat localized bone defects, even critical.

Noticeably, seeding mDPSCs within the hydrogel did not improve neither bone formation rate nor its quality compared to acellular DCH, even in the presence of the highest dose of the antibody. mDPSCs with osteogenic orientation are supposed to provide growth factors that will promote bone formation and to directly participate to bone repair by differentiating into osteoblasts[80]. However, regarding mDPSCs-seeded DCH, contradictory results are found in the literature. On one hand, efficient bone repair was achieved after mDPSCs-DCH implantation but the acellular scaffold had no significant bone healing capacity[15]. On the other hand, when the acellular DCH alone did exhibit bone repair property, the addition of mDPSCs only slightly improved bone formation[39]. Here, the DCH alone showed some bone repair ability that was greatly improved by the addition of the antibody alone. Thus, the released Scl-Ab seems to be able to favor bone formation by interacting with the host cells at the vicinity of the defect. Interestingly, another study comparing mDPSCs-seeded- and acellular bioglass-doped DCH reported higher bone formation without cells[81]. Since the bone repair property of bioglasses is also due to their ability to release bioactive species[58], they may also promote bone formation by interacting with the surrounding tissue. Noteworthy, here, in the acellular gels, scattered fragments of the implanted DCH were distinguishable and were devoid of cells whereas, in the cellularized DCH, larger fragments of hydrogels were easily distinguished, with cells oriented along the collagen fibers. This suggests that the implanted mDPSCs may

remodel the DCH and decrease its porosity, thereby delaying the mineralization process. In contrast, in the looser acellular gels, host cells may be able to rapidly invade the implanted scaffold and promote fast bone formation. Alternatively, more differentiated osteoprogenitors or bone marrow stem cells might be compared to DPSC in the future in the same model.

As a next step, it will be important to extend these experiments to more challenging in vivo conditions. This study was conducted in a flat bone, which is not exposed to strong mechanical constraints[82]. Thus our findings need to be evaluated in a more mechanically-challenged bone, such as the mandible [83], which will require stronger scaffolds such as premineralized collagen hydrogels. Furthermore, our experiments were conducted in young male mice with an important healing potential. Our study must be repeated in both males and females as, similarly to humans, female are more prone to fractures[84,85]. More challenging systemic conditions also have to be examined. Indeed, co-morbidities, such as diabetes, and poor lifestyle (smoking or alcohol abuse, inactivity) increase the risk of delayed healing and non-unions because of too poor and/or disrupted vascularization and an insufficient number of skeletal progenitor cells. It remains to be determined whether, under these more demanding conditions, (i) the local administration of the antibody still provides outcomes as positive as the systemic treatment, (ii) the presence of MSCs could improve the healing process. In parallel, increasing the Scl-Ab loading capacity of the DCH as well as achieving a better temporal control of its delivery could further enhance bone regeneration. Further improvement of the bone repair properties of the scaffold by incorporation of bioactive particles can be also foreseen.

5. Conclusion

This study demonstrates that the local delivery of an anti-sclerostin monoclonal antibody loaded in a dense collagen hydrogel can be as efficient the combination of the hydrogel with IV injection of the antibody to promote robust craniofacial bone regeneration. In our context, the addition of neural crest-derived mesenchymal stem cells did not further improve the efficiency of the antibody-loaded hydrogel. The ease of preparation and use of these biomaterials make them highly attractive candidates for rapid clinical application, particularly

for delayed bone repair after, for example, hemicraniectomy in young adults. Importantly, the success of our strategy relies on the fact that the hydrogel plays a dual role, *i.e*. a scaffold to temporary fill the bone defect and a reservoir for antibody delivery. This paves the way to the design of improved biomaterials combining intrinsic bone repair capability and ability to locally deliver monoclonal antibodies for the treatment of localized bone defects.

Fundings

This work was supported by Université Paris Cité and Sorbonne Université and the *Fondation des Gueules cassées* for URP 2496. Micro-CT device was funded by Fondation pour la Recherche Médicale (FRM DGE20111123012). Setrusumab (BPS804) was provided by Mereo Biopharma (London, UK) through a Material Transfert Agreement (MTA)

Data availability

All data are available upon request.

Declaration of Conflicting Interests

The authors declare that they have no known competing financial interests or personal relationships that could have appeared to influence the work reported in this paper.

Supporting information

Additional experimental results including dimensions of the acellular hydrogels (S1), characterization of the empty and SHAM conditions (S2), characterization by SHG of the DCH, Ld DCH (S3) and mDPSC-seeded conditions (S5), histological structures of the non-mineralized area in acellular (S4) and cell-seeded condition (S6), and Bone Mineral Density (BMD) (S7).

Acknowledgments

The authors thank Lotfi Slimani (URP2496 and PIV, Université de Paris Cité, France) for his assistance in Micro-CT acquisitions and analyses, and Julie Lesieur and Thomas Guilbert

(IMAG'IC, Institut Cochin, Paris, France) for their help with Live-Dead images and second harmonic microscope acquisitions.

References

(1) Amini, A. R.; Laurencin, C. T.; Nukavarapu, S. P. Bone Tissue Engineering: Recent Advances and Challenges. *Crit. Rev. Biomed. Eng.* **2012**, *40* (5), 363–408.

(2) Henkel, J.; Woodruff, M. A.; Epari, D. R.; Steck, R.; Glatt, V.; Dickinson, I. C.; Choong, P. F. M.; Schuetz, M. A.; Hutmacher, D. W. Bone Regeneration Based on Tissue Engineering Conceptions — A 21st Century Perspective. *Bone Res.* **2013**, *1* (3), 216–248. https://doi.org/10.4248/BR201303002.

(3) Naderi, H.; Matin, M. M.; Bahrami, A. R. Review Paper: Critical Issues in Tissue Engineering: Biomaterials, Cell Sources, Angiogenesis, and Drug Delivery Systems. *J. Biomater. Appl.* **2011**, *26* (4), 383–417. https://doi.org/10.1177/0885328211408946.

(4) Collignon, A.-M.; Lesieur, J.; Vacher, C.; Chaussain, C.; Rochefort, G. Y. Strategies Developed to Induce, Direct, and Potentiate Bone Healing. *Front. Physiol.* **2017**, *8*. https://doi.org/10.3389/fphys.2017.00927.

(5) Montoya, C.; Du, Y.; Gianforcaro, A. L.; Orrego, S.; Yang, M.; Lelkes, P. I. On the Road to Smart Biomaterials for Bone Research: Definitions, Concepts, Advances, and Outlook. *Bone Res.* **2021**, *9*, 12. https://doi.org/10.1038/s41413-020-00131-z.

(6) Maisani, M.; Pezzoli, D.; Chassande, O.; Mantovani, D. Cellularizing Hydrogel-Based Scaffolds to Repair Bone Tissue: How to Create a Physiologically Relevant Micro-Environment? *J. Tissue Eng.* **2017**, *8*, 2041731417712073. https://doi.org/10.1177/2041731417712073.

(7) Kim, H.; Kumbar, S. G.; Nukavarapu, S. P. Biomaterial-Directed Cell Behavior for Tissue Engineering. *Curr. Opin. Biomed. Eng.* **2021**, *17*, 100260. https://doi.org/10.1016/j.cobme.2020.100260.

(8) Qu, H.; Fu, H.; Han, Z.; Sun, Y. Biomaterials for Bone Tissue Engineering Scaffolds: A Review. *RSC Adv. 9* (45), 26252–26262. https://doi.org/10.1039/c9ra05214c.

(9) Koons, G. L.; Mikos, A. G. Progress in Three-Dimensional Printing with Growth Factors. *J. Control. Release Off. J. Control. Release Soc.* **2019**, *295*, 50–59. https://doi.org/10.1016/j.jconrel.2018.12.035.

(10) Rimondini, L.; Fini, M.; Giardino, R. The Microbial Infection of Biomaterials: A Challenge for Clinicians and Researchers. A Short Review. *J. Appl. Biomater. Biomech.* **2005**, *3* (1), 1–10. https://doi.org/10.1177/228080000500300101.

(11) Riool, M.; Zaat, S. A. J. Biomaterial-Associated Infection: Pathogenesis and Prevention. In *Urinary Stents: Current State and Future Perspectives*; Soria, F., Rako, D., de Graaf, P., Eds.; Springer International Publishing: Cham, 2022; pp 245–257. https://doi.org/10.1007/978-3-031-04484-7_20.

(12) Gao, C.; Peng, S.; Feng, P.; Shuai, C. Bone Biomaterials and Interactions with Stem Cells. *Bone Res.* **2017**, *5*, 17059. https://doi.org/10.1038/boneres.2017.59.

(13) Suman, S.; Domingues, A.; Ratajczak, J.; Ratajczak, M. Z. Potential Clinical Applications of Stem Cells in Regenerative Medicine. In *Stem Cells: Therapeutic Applications*; Ratajczak, M. Z., Ed.; Advances in Experimental Medicine and Biology; Springer International Publishing: Cham, 2019; pp 1–22. https://doi.org/10.1007/978-3-030-31206-0_1.

(14) Zhang, S.-Y.; Ren, J.-Y.; Yang, B. Priming Strategies for Controlling Stem Cell Fate: Applications and Challenges in Dental Tissue Regeneration. *World J. Stem Cells* **2021**, *13* (11), 1625–1646. https://doi.org/10.4252/wjsc.v13.i11.1625.

(15) Collignon, A.-M.; Castillo-Dali, G.; Gomez, E.; Guilbert, T.; Lesieur, J.; Nicoletti, A.; Acuna-Mendoza, S.; Letourneur, D.; Chaussain, C.; Rochefort, G. Y.; Poliard, A. Mouse Wnt1-CRE-RosaTomato Dental Pulp Stem Cells Directly Contribute to the Calvarial Bone Regeneration Process. *Stem Cells* **2019**, *37* (5), 701–711. https://doi.org/10.1002/stem.2973.

(16) Petrus-Reurer, S.; Romano, M.; Howlett, S.; Jones, J. L.; Lombardi, G.; Saeb-Parsy, K. Immunological Considerations and Challenges for Regenerative Cellular Therapies. *Commun. Biol.* **2021**, *4* (1), 1–16. https://doi.org/10.1038/s42003-021-02237-4.

(17) Coelho, M. B.; Cabral, J. M. S.; Karp, J. M. Intraoperative Stem Cell Therapy. *Annu. Rev. Biomed. Eng.* **2012**, *14*, 325–349. https://doi.org/10.1146/annurev-bioeng-071811-150041.
(18) Biondi, M.; Ungaro, F.; Quaglia, F.; Netti, P. A. Controlled Drug Delivery in Tissue Engineering. *Adv. Drug Deliv. Rev.* **2008**, *60* (2), 229–242. https://doi.org/10.1016/j.addr.2007.08.038.
(19) Saltzman, W. M.; Olbricht, W. L. Building Drug Delivery into Tissue Engineering Design. *Nat. Rev. Drug Discov.* **2002**, *1* (3), 177–186. https://doi.org/10.1038/nrd744.
(20) Bai, L.; Tao, G.; Feng, M.; Xie, Y.; Cai, S.; Peng, S.; Xiao, J. Hydrogel Drug Delivery Systems for Bone Regeneration. *Pharmaceutics* **2023**, *15* (5), 1334. https://doi.org/10.3390/pharmaceutics15051334.
(21) Babensee, J. E.; McIntire, L. V.; Mikos, A. G. Growth Factor Delivery for Tissue Engineering.
(22) Kyllönen, L.; D'Este, M.; Alini, M.; Eglin, D. Local Drug Delivery for Enhancing Fracture Healing in Osteoporotic Bone. *Acta Biomater.* **2015**, *11*, 412–434. https://doi.org/10.1016/j.actbio.2014.09.006.
(23) Fletcher, N. A.; Babcock, L. R.; Murray, E. A.; Krebs, M. D. Controlled Delivery of Antibodies from Injectable Hydrogels. *Mater. Sci. Eng. C* **2016**, *59*, 801–806. https://doi.org/10.1016/j.msec.2015.10.096.
(24) Chamieh, F.; Collignon, A.-M.; Coyac, B. R.; Lesieur, J.; Ribes, S.; Sadoine, J.; Llorens, A.; Nicoletti, A.; Letourneur, D.; Colombier, M.-L.; Nazhat, S. N.; Bouchard, P.; Chaussain, C.; Rochefort, G. Y. Accelerated Craniofacial Bone Regeneration through Dense Collagen Gel Scaffolds Seeded with Dental Pulp Stem Cells. *Sci. Rep.* **2016**, *6*. https://doi.org/10.1038/srep38814.
(25) Brown, R. A.; Wiseman, M.; Chuo, C.-B.; Cheema, U.; Nazhat, S. N. Ultrarapid Engineering of Biomimetic Materials and Tissues: Fabrication of Nano- and Microstructures by Plastic Compression. *Adv. Funct. Mater.* **2005**, *15* (11), 1762–1770. https://doi.org/10.1002/adfm.200500042.
(26) Bitar, M.; Salih, V.; Brown, R. A.; Nazhat, S. N. Effect of Multiple Unconfined Compression on Cellular Dense Collagen Scaffolds for Bone Tissue Engineering. *J. Mater. Sci. Mater. Med.* **2007**, *18* (2), 237–244. https://doi.org/10.1007/s10856-006-0685-1.
(27) Griffanti, G.; Nazhat, S. N. Dense Fibrillar Collagen-Based Hydrogels as Functional Osteoid-Mimicking Scaffolds. *Int. Mater. Rev.* **2020**, *65* (8), 502–521. https://doi.org/10.1080/09506608.2020.1735828.
(28) Buxton, P. G.; Bitar, M.; Gellynck, K.; Parkar, M.; Brown, R. A.; Young, A. M.; Knowles, J. C.; Nazhat, S. N. Dense Collagen Matrix Accelerates Osteogenic Differentiation and Rescues the Apoptotic Response to MMP Inhibition. *Bone* **2008**, *43* (2), 377–385. https://doi.org/10.1016/j.bone.2008.03.028.
(29) Gronthos, S.; Mankani, M.; Brahim, J.; Robey, P. G.; Shi, S. Postnatal Human Dental Pulp Stem Cells (DPSCs) in Vitro and in Vivo. *Proc. Natl. Acad. Sci. U. S. A.* **2000**, *97* (25), 13625–13630.
(30) Lumsden, A. G. S. Spatial Organization of the Epithelium and the Role of Neural Crest Cells in the Initiation of the Mammalian Tooth Germ. *Development* **1988**, *103* (Supplement), 155–169. https://doi.org/10.1242/dev.103.Supplement.155.
(31) BAL, Z.; KUSHIOKA, J.; KODAMA, J.; KAITO, T.; YOSHIKAWA, H.; KORKUSUZ, P.; KORKUSUZ, F. BMP and TGFβ Use and Release in Bone Regeneration. *Turk. J. Med. Sci.* **2020**, *50* (7), 1707–1722. https://doi.org/10.3906/sag-2003-127.
(32) Piters, E.; Boudin, E.; Van Hul, W. Wnt Signaling: A Win for Bone. *Arch. Biochem. Biophys.* **2008**, *473* (2), 112–116. https://doi.org/10.1016/j.abb.2008.03.006.
(33) Van Buchem, F. S.; Hadders, H. N.; Ubbens, R. An Uncommon Familial Systemic Disease of the Skeleton: Hyperostosis Corticalis Generalisata Familiaris. *Acta Radiol.* **1955**, *44* (2), 109–120.
(34) Balemans, W.; Ebeling, M.; Patel, N.; Van Hul, E.; Olson, P.; Dioszegi, M.; Lacza, C.; Wuyts, W.; Van Den Ende, J.; Willems, P.; Paes-Alves, A. F.; Hill, S.; Bueno, M.; Ramos, F. J.; Tacconi, P.; Dikkers, F. G.; Stratakis, C.; Lindpaintner, K.; Vickery, B.; Foernzler, D.; Van Hul, W. Increased Bone Density in Sclerosteosis Is Due to the Deficiency of a Novel Secreted Protein (SOST). *Hum. Mol. Genet.* **2001**, *10* (5), 537–543.

(35) Fabre, S.; Funck-Brentano, T.; Cohen-Solal, M. Anti-Sclerostin Antibodies in Osteoporosis and Other Bone Diseases. *J. Clin. Med.* **2020**, *9* (11), 3439. https://doi.org/10.3390/jcm9113439.
(36) Glorieux, F. H.; Devogelaer, J.-P.; Durigova, M.; Goemaere, S.; Hemsley, S.; Jakob, F.; Junker, U.; Ruckle, J.; Seefried, L.; Winkle, P. J. BPS804 Anti-Sclerostin Antibody in Adults With Moderate Osteogenesis Imperfecta: Results of a Randomized Phase 2a Trial. *J. Bone Miner. Res.* **2017**, *32* (7), 1496–1504. https://doi.org/10.1002/jbmr.3143.
(37) Virk, M. S.; Alaee, F.; Tang, H.; Ominsky, M. S.; Ke, H. Z.; Lieberman, J. R. Systemic Administration of Sclerostin Antibody Enhances Bone Repair in a Critical-Sized Femoral Defect in a Rat Model. *J. Bone Joint Surg. Am.* **2013**, *95* (8), 694–701. https://doi.org/10.2106/JBJS.L.00285.
(38) Li, M.; Li, S.; Liu, J.; Cui, X.; Zhang, S.; Zhou, J.; Wang, X.; Yao, Q. Sustained-release of Sclerostin Single-chain Antibody Fragments Using Poly(Lactic-co-glycolic Acid) Microspheres for Osteoporotic Fracture Repair. *J. Biomed. Mater. Res. A* **2019**, *107* (8), 1832–1840. https://doi.org/10.1002/jbm.a.36704.
(39) Maillard, S.; Sicard, L.; Andrique, C.; Torrens, C.; Lesieur, J.; Baroukh, B.; Coradin, T.; Poliard, A.; Slimani, L.; Chaussain, C. Combining Sclerostin Neutralization with Tissue Engineering: An Improved Strategy for Craniofacial Bone Repair. *Acta Biomater.* **2022**, *140*, 178–189. https://doi.org/10.1016/j.actbio.2021.11.046.
(40) Awwad, S.; Angkawinitwong, U. Overview of Antibody Drug Delivery. *Pharmaceutics* **2018**, *10* (3), 83. https://doi.org/10.3390/pharmaceutics10030083.
(41) Chen, Z.; Kankala, R. K.; Yang, Z.; Li, W.; Xie, S.; Li, H.; Chen, A.-Z.; Zou, L. Antibody-Based Drug Delivery Systems for Cancer Therapy: Mechanisms, Challenges, and Prospects. *Theranostics* **2022**, *12* (8), 3719–3746. https://doi.org/10.7150/thno.72594.
(42) Gréa, T.; Jacquot, G.; Durand, A.; Mathieu, C.; Gasser, A.; Zhu, C.; Banerjee, M.; Hucteau, E.; Mallard, J.; Lopez Navarro, P.; Popescu, B. V.; Thomas, E.; Kryza, D.; Sidi-Boumedine, J.; Ferrauto, G.; Gianolio, E.; Fleith, G.; Combet, J.; Brun, S.; Erb, S.; Cianferani, S.; Charbonnière, L. J.; Fellmann, L.; Mirjolet, C.; David, L.; Tillement, O.; Lux, F.; Harlepp, S.; Pivot, X.; Detappe, A. Subcutaneous Administration of a Zwitterionic Chitosan-Based Hydrogel for Controlled Spatiotemporal Release of Monoclonal Antibodies. *Adv. Mater. n/a* (n/a), 2308738. https://doi.org/10.1002/adma.202308738.
(43) Kasse, C. M.; Yu, A. C.; Powell, A. E.; Roth, G. A.; Liong, C. S.; Jons, C. K.; Buahin, A.; Maikawa, C. L.; Zhou, X.; Youssef, S.; Glanville, J. E.; Appel, E. A. Subcutaneous Delivery of an Antibody against SARS-CoV-2 from a Supramolecular Hydrogel Depot. *Biomater. Sci. 11* (6), 2065–2079. https://doi.org/10.1039/d2bm00819j.
(44) Coyac, B. R.; Chicatun, F.; Hoac, B.; Nelea, V.; Chaussain, C.; Nazhat, S. N.; McKee, M. D. Mineralization of Dense Collagen Hydrogel Scaffolds by Human Pulp Cells. *J. Dent. Res.* **2013**, *92* (7), 648–654. https://doi.org/10.1177/0022034513488599.
(45) Rajan, N.; Habermehl, J.; Coté, M.-F.; Doillon, C. J.; Mantovani, D. Preparation of Ready-to-Use, Storable and Reconstituted Type I Collagen from Rat Tail Tendon for Tissue Engineering Applications. *Nat. Protoc.* **2006**, *1* (6), 2753–2758. https://doi.org/10.1038/nprot.2006.430.
(46) Schindelin, J.; Arganda-Carreras, I.; Frise, E.; Kaynig, V.; Longair, M.; Pietzsch, T.; Preibisch, S.; Rueden, C.; Saalfeld, S.; Schmid, B.; Tinevez, J.-Y.; White, D. J.; Hartenstein, V.; Eliceiri, K.; Tomancak, P.; Cardona, A. Fiji: An Open-Source Platform for Biological-Image Analysis. *Nat. Methods* **2012**, *9* (7), 676–682. https://doi.org/10.1038/nmeth.2019.
(47) Murphy, M. P.; Quarto, N.; Longaker, M. T.; Wan, D. C. Calvarial Defects: Cell-Based Reconstructive Strategies in the Murine Model. *Tissue Eng. Part C Methods* **2017**, *23* (12), 971–981. https://doi.org/10.1089/ten.tec.2017.0230.
(48) Bouxsein, M. L.; Boyd, S. K.; Christiansen, B. A.; Guldberg, R. E.; Jepsen, K. J.; Müller, R. Guidelines for Assessment of Bone Microstructure in Rodents Using Micro–Computed Tomography. *J. Bone Miner. Res.* **2010**, *25* (7), 1468–1486. https://doi.org/10.1002/jbmr.141.
(49) Lafont, J.; Baroukh, B.; Berdal, A.; Colombier, M. L.; Barritault, D.; Caruelle, J. P.; Saffar, J. L. RGTA11, a New Healing Agent, Triggers Developmental Events during Healing of Craniotomy

Defects in Adult Rats. *Growth Factors* **1998**, *16* (1), 23–38. https://doi.org/10.3109/08977199809017489.
(50) Guilbert, T.; Odin, C.; Grand, Y. L.; Gailhouste, L.; Turlin, B.; Ezan, F.; Désille, Y.; Baffet, G.; Guyader, D. A Robust Collagen Scoring Method for Human Liver Fibrosis by Second Harmonic Microscopy. *Opt. Express* **2010**, *18* (25), 25794–25807. https://doi.org/10.1364/OE.18.025794.
(51) Connolly, C.; Sabarigirivasan, V.; Cottone, L.; Flanagan, A. M.; Tirabosco, R. An Overview and Update on Bone Lesion in Craniofacial Bones. *Diagn. Histopathol.* **2021**, *27* (5), 216–225. https://doi.org/10.1016/j.mpdhp.2021.02.006.
(52) Emara, A.; Shah, R. Recent Update on Craniofacial Tissue Engineering. *J. Tissue Eng.* **2021**, *12*, 20417314211003735. https://doi.org/10.1177/20417314211003735.
(53) Zhang, W.; Yelick, P. C. Craniofacial Tissue Engineering. *Cold Spring Harb. Perspect. Med.* **2018**, *8* (1), a025775. https://doi.org/10.1101/cshperspect.a025775.
(54) Center for Drug Evaluation and Research. Drug Trials Snapshot: EVENITY. *FDA* **2019**.
(55) *Evenity | European Medicines Agency*. https://www.ema.europa.eu/en/medicines/human/EPAR/evenity (accessed 2024-03-10).
(56) Rico-Llanos, G. A.; Borrego-González, S.; Moncayo-Donoso, M.; Becerra, J.; Visser, R. Collagen Type I Biomaterials as Scaffolds for Bone Tissue Engineering. *Polymers* **2021**, *13* (4), 599. https://doi.org/10.3390/polym13040599.
(57) Wang, Y.; Wang, Z.; Dong, Y. Collagen-Based Biomaterials for Tissue Engineering. *ACS Biomater. Sci. Eng.* **2023**, *9* (3), 1132–1150. https://doi.org/10.1021/acsbiomaterials.2c00730.
(58) Sarker, B.; Hum, J.; Nazhat, S. N.; Boccaccini, A. R. Combining Collagen and Bioactive Glasses for Bone Tissue Engineering: A Review. *Adv. Healthc. Mater.* **2015**, *4* (2), 176–194. https://doi.org/10.1002/adhm.201400302.
(59) Friess, W. Collagen – Biomaterial for Drug Delivery. *Eur. J. Pharm. Biopharm.* **1998**.
(60) Helary, C.; Abed, A.; Mosser, G.; Louedec, L.; Letourneur, D.; Coradin, T.; Giraud-Guille, M. M.; Meddahi-Pellé, A. Evaluation of Dense Collagen Matrices as Medicated Wound Dressing for the Treatment of Cutaneous Chronic Wounds. *Biomater. Sci.* **2015**, *3* (2), 373–382. https://doi.org/10.1039/C4BM00370E.
(61) Wallace, D. G.; Rosenblatt, J. Collagen Gel Systems for Sustained Delivery and Tissue Engineering. *Adv. Drug Deliv. Rev.* **2003**, *55* (12), 1631–1649. https://doi.org/10.1016/j.addr.2003.08.004.
(62) Lin, K.; Zhang, D.; Macedo, M. H.; Cui, W.; Sarmento, B.; Shen, G. Advanced Collagen-Based Biomaterials for Regenerative Biomedicine. *Adv. Funct. Mater.* **2019**, *29* (3), 1804943. https://doi.org/10.1002/adfm.201804943.
(63) Helary, C.; Abed, A.; Mosser, G.; Louedec, L.; Meddahi-Pellé, A.; Giraud-Guille, M. M. Synthesis and in Vivo Integration of Improved Concentrated Collagen Hydrogels. *J. Tissue Eng. Regen. Med.* **2011**, *5* (3), 248–252. https://doi.org/10.1002/term.326.
(64) Cross, V. L.; Zheng, Y.; Choi, N. W.; Verbridge, S. S.; Sutermaster, B. A.; Bonassar, L. J.; Fischbach, C.; Stroock, A. D. Dense Type I Collagen Matrices That Support Cellular Remodeling and Microfabrication for Studies of Tumor Angiogenesis and Vasculogenesis in Vitro. *Biomaterials* **2010**, *31* (33), 8596–8607. https://doi.org/10.1016/j.biomaterials.2010.07.072.
(65) Mbitta Akoa, D.; Sicard, L.; Hélary, C.; Torrens, C.; Baroukh, B.; Poliard, A.; Coradin, T. Role of Physico-Chemical and Cellular Conditions on the Bone Repair Potential of Plastically Compressed Collagen Hydrogels. *Gels* **2024**, *10* (2), 130. https://doi.org/10.3390/gels10020130.
(66) Levis, H. J.; Brown, R. A.; Daniels, J. T. Plastic Compressed Collagen as a Biomimetic Substrate for Human Limbal Epithelial Cell Culture. *Biomaterials* **2010**, *31* (30), 7726–7737. https://doi.org/10.1016/j.biomaterials.2010.07.012.
(67) East, E.; de Oliveira, D. B.; Golding, J. P.; Phillips, J. B. Alignment of Astrocytes Increases Neuronal Growth in Three-Dimensional Collagen Gels and Is Maintained Following Plastic Compression to Form a Spinal Cord Repair Conduit. *Tissue Eng. Part A* **2010**, *16* (10), 3173–3184. https://doi.org/10.1089/ten.tea.2010.0017.

(68) Rosenzweig, D. H.; Chicatun, F.; Nazhat, S. N.; Quinn, T. M. Cartilaginous Constructs Using Primary Chondrocytes from Continuous Expansion Culture Seeded in Dense Collagen Gels. *Acta Biomater.* **2013**, *9* (12), 9360–9369. https://doi.org/10.1016/j.actbio.2013.07.024.
(69) Pavlou, M.; Shah, M.; Gikas, P.; Briggs, T.; Roberts, S. J.; Cheema, U. Osteomimetic Matrix Components Alter Cell Migration and Drug Response in a 3D Tumour-Engineered Osteosarcoma Model. *Acta Biomater.* **2019**, *96*, 247–257. https://doi.org/10.1016/j.actbio.2019.07.011.
(70) Haugh, M. G.; Thorpe, S. D.; Vinardell, T.; Buckley, C. T.; Kelly, D. J. The Application of Plastic Compression to Modulate Fibrin Hydrogel Mechanical Properties. *J. Mech. Behav. Biomed. Mater.* **2012**, *16*, 66–72. https://doi.org/10.1016/j.jmbbm.2012.10.009.
(71) Brown, R. A.; Wiseman, M.; Chuo, C.-B.; Cheema, U.; Nazhat, S. N. Ultrarapid Engineering of Biomimetic Materials and Tissues: Fabrication of Nano- and Microstructures by Plastic Compression. *Adv. Funct. Mater.* **2005**, *15* (11), 1762–1770. https://doi.org/10.1002/adfm.200500042.
(72) Jurczak, P.; Lach, S. Hydrogels as Scaffolds in Bone-Related Tissue Engineering and Regeneration. *Macromol. Biosci.* **2023**, *23* (11), 2300152. https://doi.org/10.1002/mabi.202300152.
(73) Weitkamp, J.-T.; Benz, K.; Rolauffs, B.; Bayer, A.; Weuster, M.; Lucius, R.; Gülses, A.; Naujokat, H.; Wiltfang, J.; Lippross, S.; Hoffmann, M.; Kurz, B.; Behrendt, P. In Vitro Comparison of 2 Clinically Applied Biomaterials for Autologous Chondrocyte Implantation: Injectable Hydrogel Versus Collagen Scaffold. *Cartilage* **2023**, *14* (2), 220–234. https://doi.org/10.1177/19476035231154507.
(74) Erickson, C. B.; Newsom, J. P.; Fletcher, N. A.; Feuer, Z. M.; Yu, Y.; Rodriguez-Fontan, F.; Hadley Miller, N.; Krebs, M. D.; Payne, K. A. In Vivo Degradation Rate of Alginate–Chitosan Hydrogels Influences Tissue Repair Following Physeal Injury. *J. Biomed. Mater. Res. B Appl. Biomater.* **2020**, *108* (6), 2484–2494. https://doi.org/10.1002/jbm.b.34580.
(75) Szekalska, M.; Puciłowska, A.; Szymańska, E.; Ciosek, P.; Winnicka, K. Alginate: Current Use and Future Perspectives in Pharmaceutical and Biomedical Applications. *Int. J. Polym. Sci.* **2016**, *2016* (1), 7697031. https://doi.org/10.1155/2016/7697031.
(76) Nunamaker, E. A.; Kipke, D. R. An Alginate Hydrogel Dura Mater Replacement for Use with Intracortical Electrodes. *J. Biomed. Mater. Res. B Appl. Biomater.* **2010**, *95B* (2), 421–429. https://doi.org/10.1002/jbm.b.31733.
(77) Callovini, G. M.; Bolognini, A.; Callovini, T.; Giordano, M.; Gazzeri, R. Treatment of CSF Leakage and Infections of Dural Substitute in Decompressive Craniectomy Using Fascia Lata Implants and Related Anatomopathological Findings. *Br. J. Neurosurg.* **2021**, *35* (1), 18–21. https://doi.org/10.1080/02688697.2020.1735301.
(78) McColm, J.; Hu, L.; Womack, T.; Tang, C. C.; Chiang, A. Y. Single- and Multiple-Dose Randomized Studies of Blosozumab, a Monoclonal Antibody Against Sclerostin, in Healthy Postmenopausal Women: STUDIES OF BLOSOZUMAB IN POSTMENOPAUSAL WOMEN. *J. Bone Miner. Res.* **2014**, *29* (4), 935–943. https://doi.org/10.1002/jbmr.2092.
(79) Padhi, D.; Jang, G.; Stouch, B.; Fang, L.; Posvar, E. Single-Dose, Placebo-Controlled, Randomized Study of AMG 785, a Sclerostin Monoclonal Antibody. *J. Bone Miner. Res.* **2011**, *26* (1), 19–26. https://doi.org/10.1002/jbmr.173.
(80) Morad, G.; Kheiri, L.; Khojasteh, A. Dental Pulp Stem Cells for in Vivo Bone Regeneration: A Systematic Review of Literature. *Arch. Oral Biol.* **2013**, *58* (12), 1818–1827. https://doi.org/10.1016/j.archoralbio.2013.08.011.
(81) Park, H.; Collignon, A.-M.; Lepry, W. C.; Ramirez-GarciaLuna, J. L.; Rosenzweig, D. H.; Chaussain, C.; Nazhat, S. N. Acellular Dense Collagen-S53P4 Bioactive Glass Hybrid Gel Scaffolds Form More Bone than Stem Cell Delivered Constructs. *Mater. Sci. Eng. C* **2021**, *120*, 111743. https://doi.org/10.1016/j.msec.2020.111743.
(82) Lipphaus, A.; Witzel, U. Three-Dimensional Finite Element Analysis of the Dural Folds and the Human Skull under Head Acceleration. *Anat. Rec.* **2021**, *304* (2), 384–392. https://doi.org/10.1002/ar.24401.

(83) Meyer, C.; Kahn, J.-L.; Boutemy, P.; Wilk, A. Determination of the External Forces Applied to the Mandible during Various Static Chewing Tasks. *J. Cranio-Maxillofac. Surg.* **1998**, *26* (5), 331–341. https://doi.org/10.1016/S1010-5182(98)80064-4.

(84) Bergh, C.; Wennergren, D.; Möller, M.; Brisby, H. Fracture Incidence in Adults in Relation to Age and Gender: A Study of 27,169 Fractures in the Swedish Fracture Register in a Well-Defined Catchment Area. *PLoS ONE* **2020**, *15* (12), e0244291. https://doi.org/10.1371/journal.pone.0244291.

(85) Wu, A.-M.; Bisignano, C.; James, S. L.; Abady, G. G.; Abedi, A.; Abu-Gharbieh, E.; Alhassan, R. K.; Alipour, V.; Arabloo, J.; Asaad, M.; Asmare, W. N.; Awedew, A. F.; Banach, M.; Banerjee, S. K.; Bijani, A.; Birhanu, T. T. M.; Bolla, S. R.; Cámera, L. A.; Chang, J.-C.; Cho, D. Y.; Chung, M. T.; Couto, R. A. S.; Dai, X.; Dandona, L.; Dandona, R.; Farzadfar, F.; Filip, I.; Fischer, F.; Fomenkov, A. A.; Gill, T. K.; Gupta, B.; Haagsma, J. A.; Haj-Mirzaian, A.; Hamidi, S.; Hay, S. I.; Ilic, I. M.; Ilic, M. D.; Ivers, R. Q.; Jürisson, M.; Kalhor, R.; Kanchan, T.; Kavetskyy, T.; Khalilov, R.; Khan, E. A.; Khan, M.; Kneib, C. J.; Krishnamoorthy, V.; Kumar, G. A.; Kumar, N.; Lalloo, R.; Lasrado, S.; Lim, S. S.; Liu, Z.; Manafi, A.; Manafi, N.; Menezes, R. G.; Meretoja, T. J.; Miazgowski, B.; Miller, T. R.; Mohammad, Y.; Mohammadian-Hafshejani, A.; Mokdad, A. H.; Murray, C. J. L.; Naderi, M.; Naimzada, M. D.; Nayak, V. C.; Nguyen, C. T.; Nikbakhsh, R.; Olagunju, A. T.; Otstavnov, N.; Otstavnov, S. S.; Padubidri, J. R.; Pereira, J.; Pham, H. Q.; Pinheiro, M.; Polinder, S.; Pourchamani, H.; Rabiee, N.; Radfar, A.; Rahman, M. H. U.; Rawaf, D. L.; Rawaf, S.; Saeb, M. R.; Samy, A. M.; Riera, L. S.; Schwebel, D. C.; Shahabi, S.; Shaikh, M. A.; Soheili, A.; Tabarés-Seisdedos, R.; Tovani-Palone, M. R.; Tran, B. X.; Travillian, R. S.; Valdez, P. R.; Vasankari, T. J.; Velazquez, D. Z.; Venketasubramanian, N.; Vu, G. T.; Zhang, Z.-J.; Vos, T. Global, Regional, and National Burden of Bone Fractures in 204 Countries and Territories, 1990–2019: A Systematic Analysis from the Global Burden of Disease Study 2019. *Lancet Healthy Longev.* **2021**, *2* (9), e580–e592. https://doi.org/10.1016/S2666-7568(21)00172-0.

Figure legends.

Figure 1. Characterization of the collagen hydrogel before and after compression, distribution, loading capacity and release kinetics of Sclerostin-antibody. A: View in two-dimensions of the segmentation of a radio-dense hydrogel (addition of barium sulfate) before (left) and after (right) compression, showing that the hydrogel thickness is decreased but its diameter is preserved. **B**: Volume of the hydrogels after and before compression, indicating a 6-fold decreased (mm^3, n=8). **C:** SEM images of the collagen hydrogel before and after compression, highlighting a decrease in porosity with no modification of fiber morphology. **D:** confocal imaging of Hd DCH with 5% labelled Scl-Ab showing clusters and focal points well-distributed all over the DCH (n=1). **E**: Scl-Ab loading in DCHs as a function of Scl-Ab mass in the initial solution, suggesting that the maximum loading capacity is reached for a starting 2 $mg.mL^{-1}$ concentration (n=2 gels/condition). **F**: Release kinetics profile of Scl-Ab from DCHs with two different loadings, showing a rapid release over the first *ca*. 10 hours (n=3 gels for 2 $mg.mL^{-1}$ condition, 2 gels for 0.2 $mg.mL^{-1}$ condition, no significant difference at each time for each condition).

Figure 2: Evaluation of bone repair in the presence of Sclerostin antibody-loaded dense collagen hydrogels. **A:** Representative three-dimensional images of bone defects created in mice calvaria, in four conditions: left empty, filled with acellular hydrogel and filled with acellular Scl-Ab loaded (initial concentration: Ld: 0.2 $mg.mL^{-1}$, Hd: 2 $mg.mL^{-1}$) hydrogels after 30 days (D30, light color) and 60 days (D60, deep color), revealing an almost complete closure at D60 for Hd DCH. **B-C**: BV/TV (**B)** and porosity **(C)** evolution at 0, 30 and 60 days showing a significant difference at day 60 between the Hd DCH condition (n=14) and the empty (n=6), DCH alone (n=12) and Ld DCH (n=16) conditions. **D**: Masson's trichrome staining of a whole defect (coronal orientation) and magnified inserts (scale bar: 200 µm). Light blue: remaining DCH, acellular; Green blue: Bone structure with organized layer of collagen, including osteocytes and vascularization (empty condition not shown, available in FigS2). E: SHG of a whole defect (coronal orientation) and a magnified insert of the Hd DCH condition. White arrow: organized layers of collagen **F**: Von Kossa, ALP and TRAP staining of representative histological sections. Whole defect (coronal orientation) (Von Kossa staining, scale bar: 200 µm) and magnified inserts (scale bar: 20 µm) showing the presence of a functional bone with

mineralized tissue (Von Kossa staining), osteoblast activity (ALP, purple staining), and osteoclast activity (TRAP, red staining). Red arrows: osteoblasts associated to osteoid matrix (light purple on Von Kossa).

Figure 3: Evaluation of bone repair in the presence of dense collagen hydrogels seeded with mDPSCs, with or without Sclerostin antibody. A: Representative three-dimensional images of bone defects created in mice calvaria, in four conditions: filled with acellular Hd DCH and filled with *mDPSCs*-seeded unloaded DCH, Ld DCH and Hd DCH after 30 days (D30, light color) and 60 days (D60, deep color), revealing limited bone formation at D60 for all cellularized hydrogels. **B-C:** BV/TV (**B**) and porosity (**C**) evolution at 0, 30 and 60 days showing a significantly lower repair for cellularized hydrogels (n=12, 10 and 14 for mDPSCs, mDPSCs-Ld DCH and mDPSCs-Hd DCH conditions, respectively) compared to the acellular Hd DCH condition (n=12). **D**: Masson's trichrome staining of a whole defect (coronal orientation) and magnified inserts (scale bar: 200 µm), showing the presence of a bony structure with organized layers of collagen, including osteocytes and few intra vascularization (only visible in the Hd DCH and mDPSCs-Ld DCH conditions). **E**: Von Kossa, ALP and TRAP staining of representative histological sections. Whole defect (coronal orientation) (Von Kossa staining) and magnified inserts (scale bar: 200 µm), showing the presence of a functional bone with mineralized tissue (Von Kossa staining), osteoclast activity (TRAP, red staining) and osteoblast activity (ALP, purple staining).

Figure 4: In vitro characterization of dense collagen hydrogels seeded with Dental Pulp Stem Cells and loaded with Sclerostin antibody. A: Live/Dead images of mDPSCs within unloaded DCH, Ld-DCH and Hd-DCH after 24 h of culture. Green and red colors are for alive and dead cells, respectively. Scale bar: 2 mm. Magnified insets (x4, 500 µm*500 µm) showing homogeneous repartition of the living and dead cells in all conditions. **B**: Cell death ratio, as calculated from the Live/Dead assay, indicating no significant difference after 24 hours of culture among all conditions. **C:** Extent of Alamar Blue reagent reduction showing no significant difference after 28 days of culture among all conditions. **D**: Cumulative release of

Scl-Ab from Hd DCH with or without seeded mDPSCs, suggesting no significant difference between the two conditions.

Figure 5: Comparison of bone repair in local or systemic dispensation of the Sclerostin antibody. A: Representative three-dimensional images of bone defects created in mice calvaria, in two conditions: filled with acellular hydrogels loaded at high dose (Hd DCH) and filled with acellular unloaded hydrogels combined with weekly Scl Ab IV injection (inj), after 30 days (D30, light color) and 60 days (D60, deep color) revealing nearly complete closure in both conditions at 60 days. **B-C**: BV/TV (**B**) and porosity (**C**) evolution at 30 and 60 days showing no significant difference between Hd DCH (n=16) and DCH + inj (n=12) conditions (Dotted line, sham surgery). **D**: Masson's trichrome staining showing a whole defect (coronal orientation) and magnified inserts (Scale bar: 200 µm), showing the presence of a bony structure with organized layers of collagen, including osteocytes and vascularization. **E**: Von Kossa, ALP and TRAP staining of representative histological sections (Scale bar: 50 µm), showing the presence of a functional bone with mineralized tissue (Von Kossa staining), high osteoblast activity (ALP, purple staining), and low osteoclast activity (TRAP, red staining). **F**: SHG of a whole defect (coronal orientation) and a magnified insert of the Hd DCH and DCH + inj conditions. Fibrillar collagen is enhanced in red (Scale bar: 200µm).

TOC Graphic

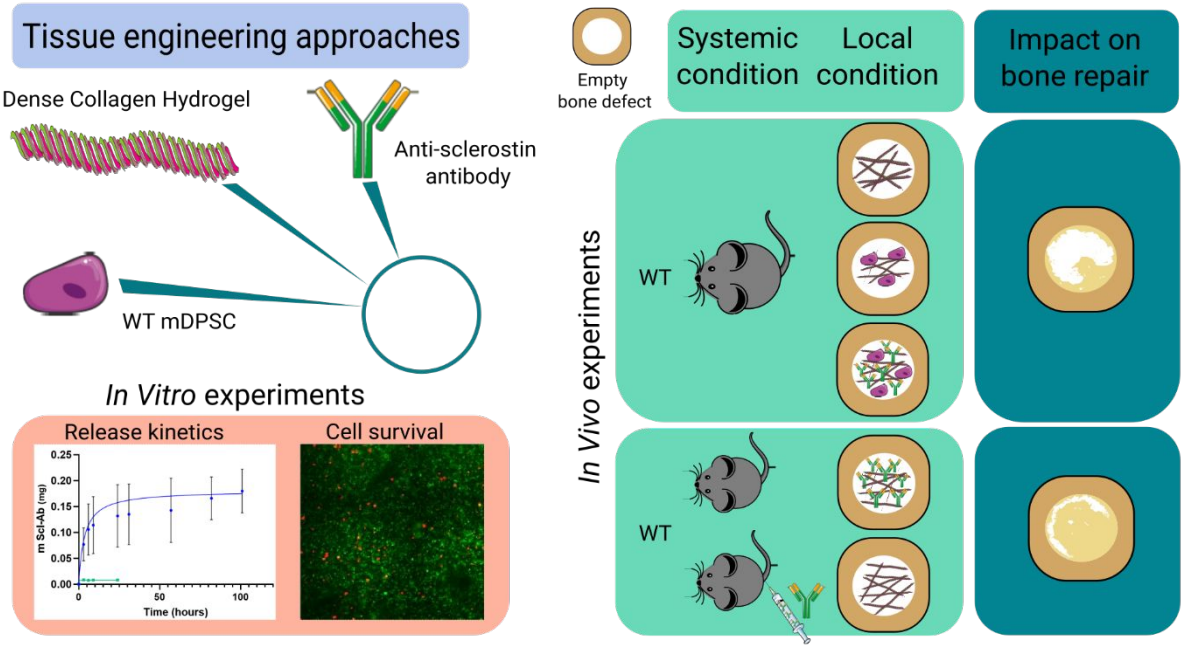
Tissue engineering approaches
Dense Collagen Hydrogel
Anti-sclerostin antibody
WT mDPSC
In Vitro experiments
Release kinetics
Cell survival
m Scl-Ab (mg)
Time (hours)
Empty bone defect
Systemic condition
Local condition
Impact on bone repair
In Vivo experiments
WT
WT

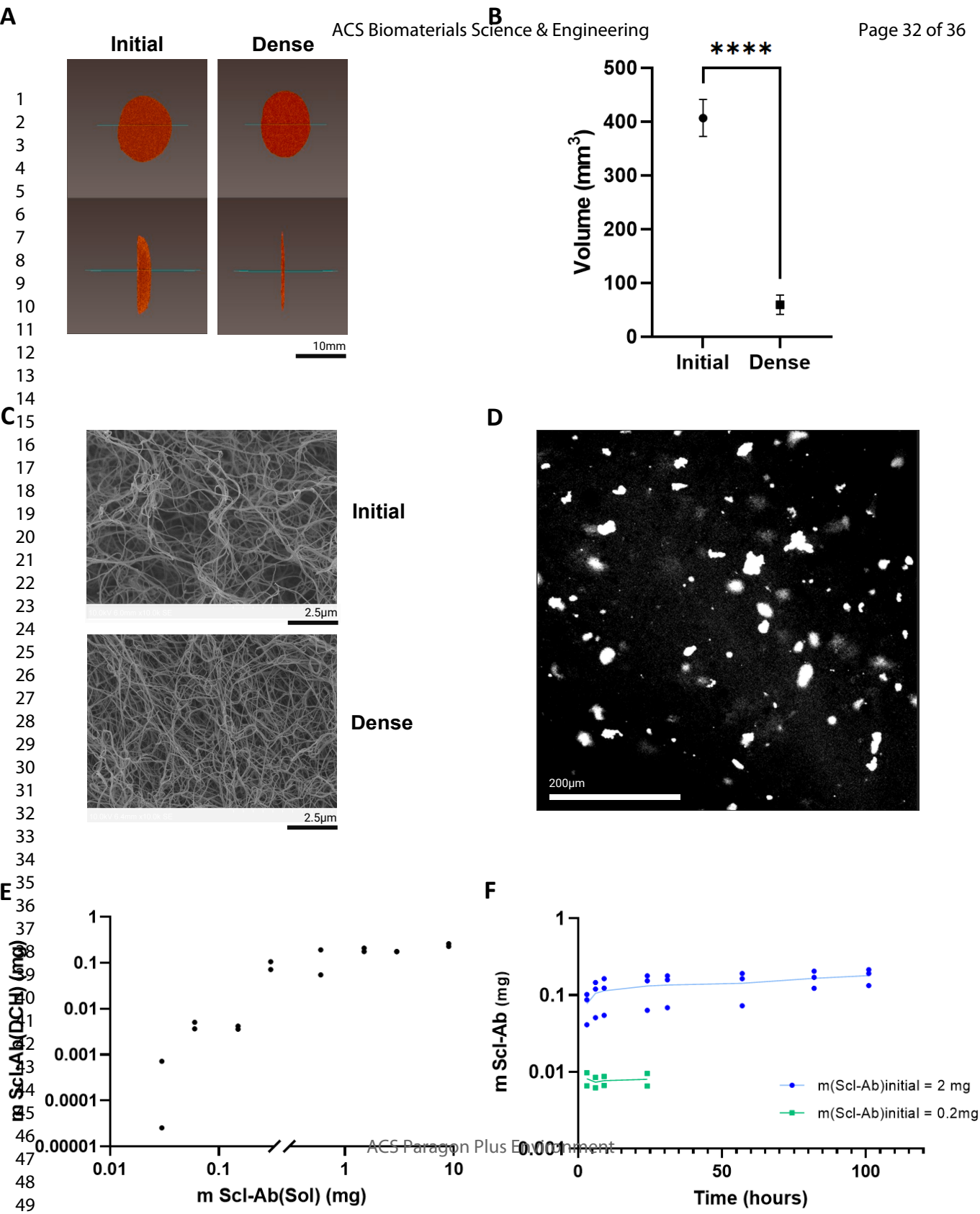

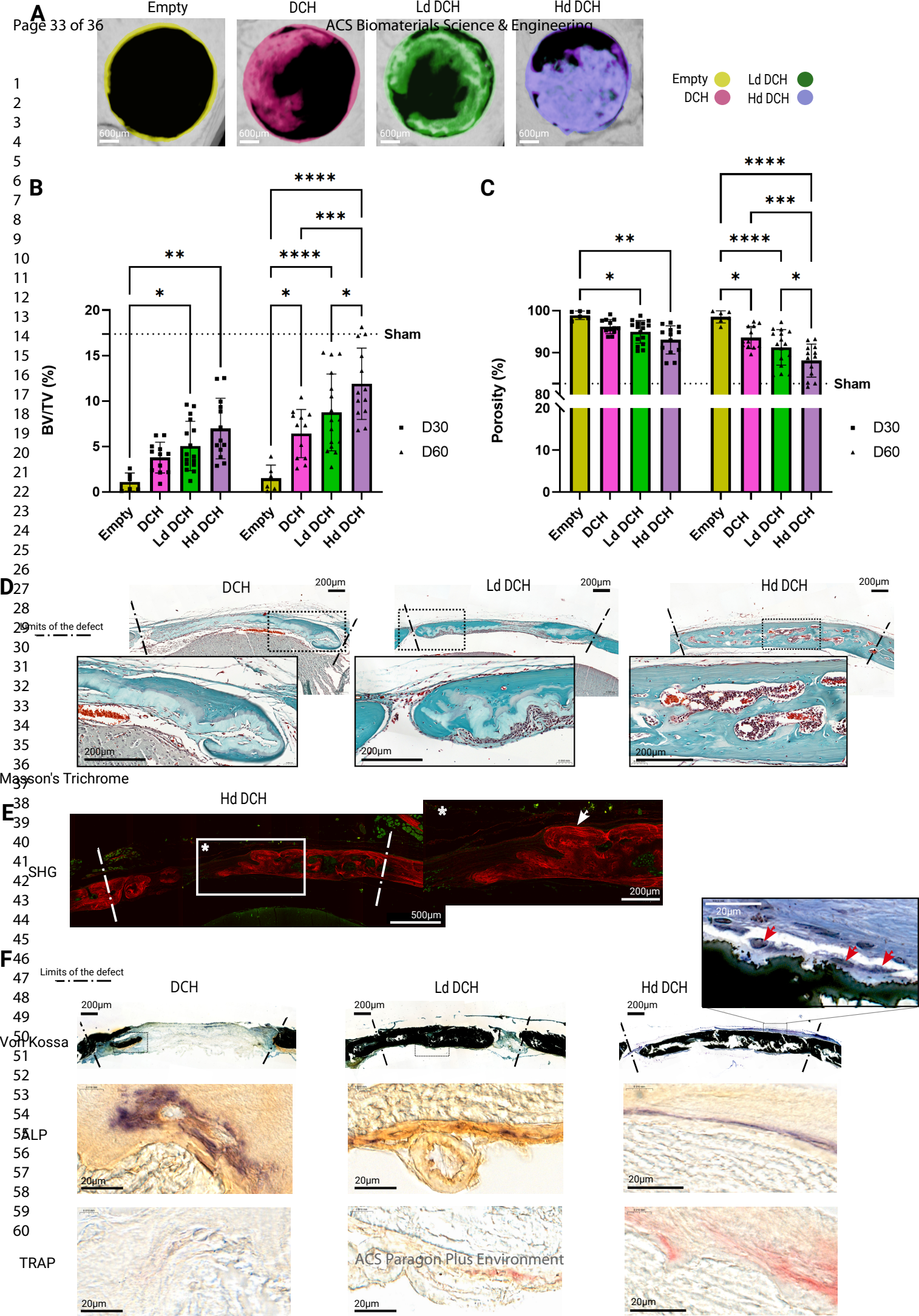
A
Empty
DCH
Ld DCH
Hd DCH
600µm
Empty
DCH
Ld DCH
Hd DCH
B
BV/TV (%)
Sham
D30
D60
Empty
DCH
Ld DCH
Hd DCH
C
Porosity (%)
Sham
D30
D60
D
DCH
Ld DCH
Hd DCH
200µm
Limits of the defect
Masson's Trichrome
E
Hd DCH
SHG
500µm
200µm
20µm
F
Limits of the defect
DCH
Ld DCH
Hd DCH
200µm
Von Kossa
ALP
TRAP
20µm
ACS Paragon Plus Environment

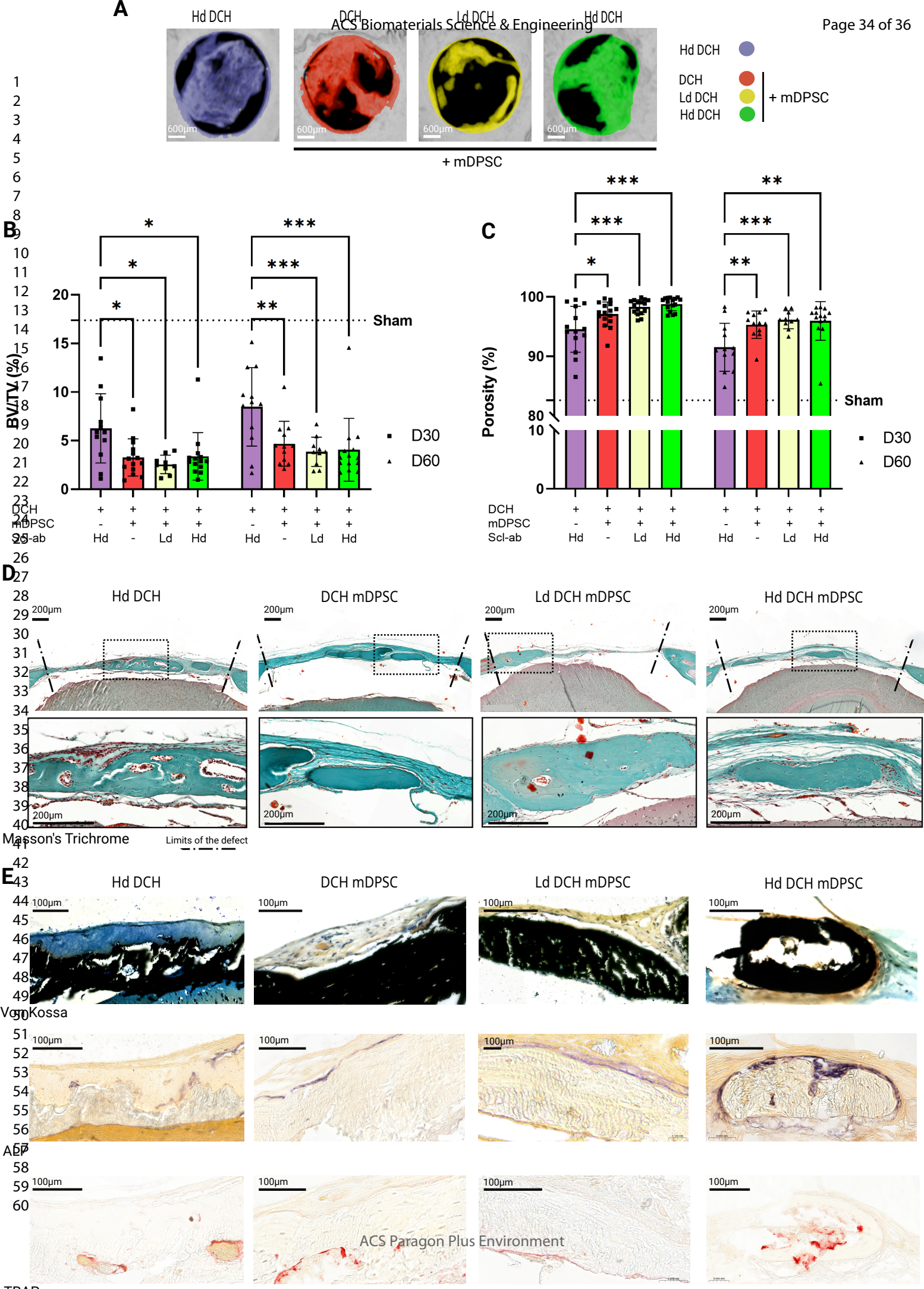

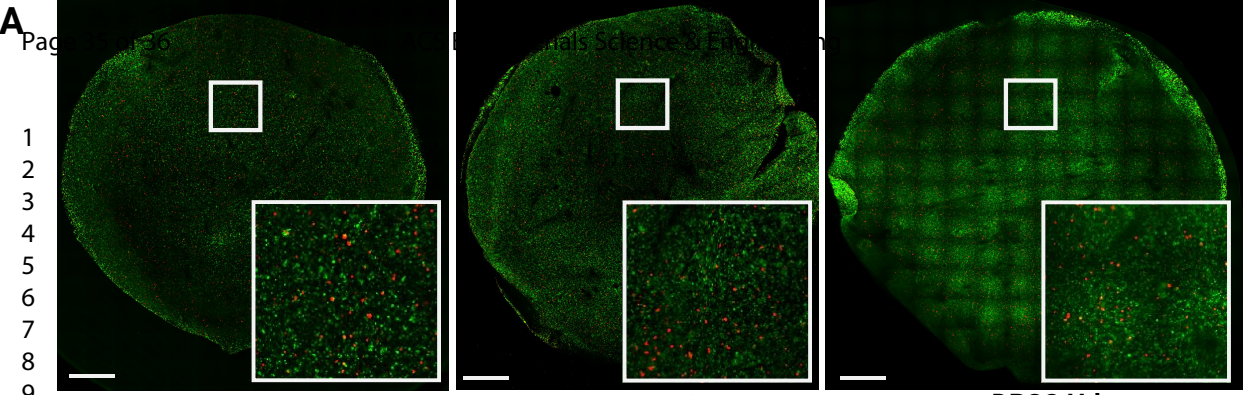

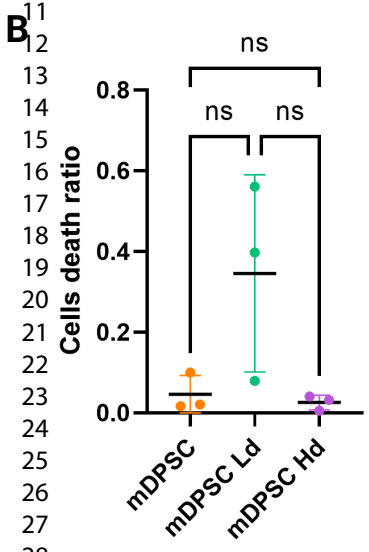

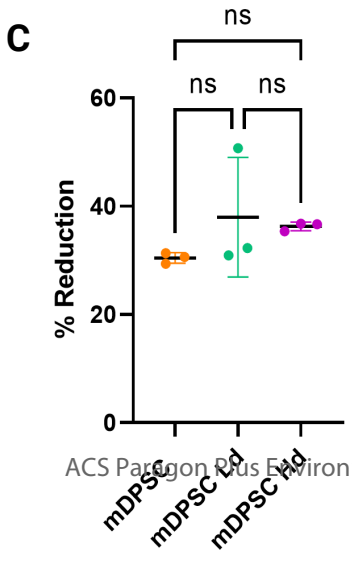

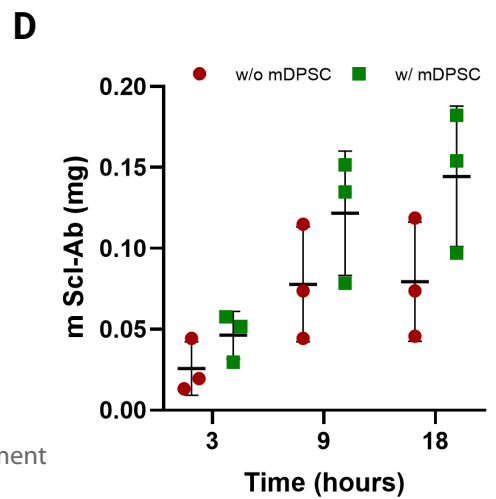

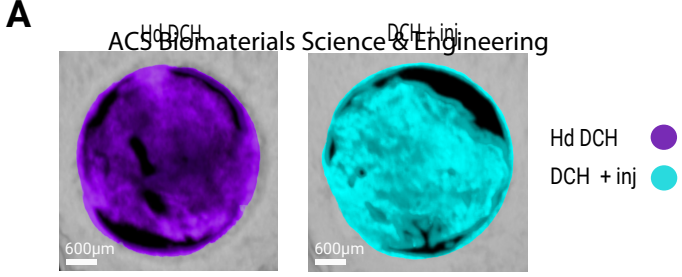
A
Hd DCH
DCH + inj
600µm
600µm
Hd DCH
DCH + inj

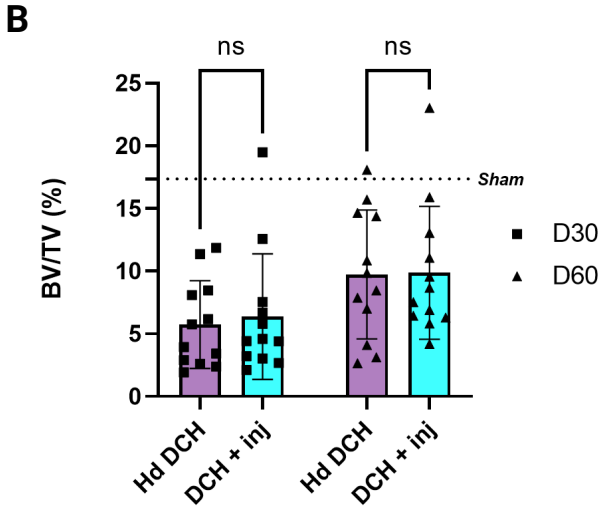
B
ns
ns
BV/TV (%)
25
20
15
10
5
0
Sham
D30
D60
Hd DCH
DCH + inj
Hd DCH
DCH + inj

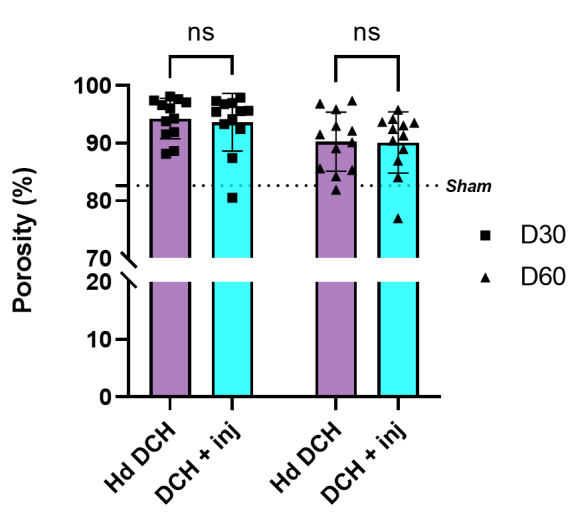
C
ns
ns
Porosity (%)
100
90
80
70
20
10
0
Sham
D30
D60
Hd DCH
DCH + inj
Hd DCH
DCH + inj

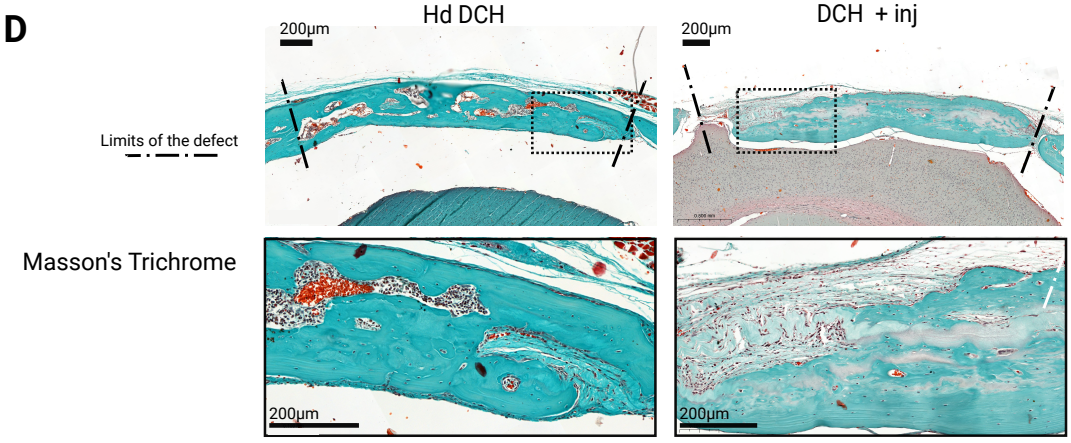
D
Hd DCH
DCH + inj
200µm
200µm
Limits of the defect
Masson's Trichrome
200µm
200µm

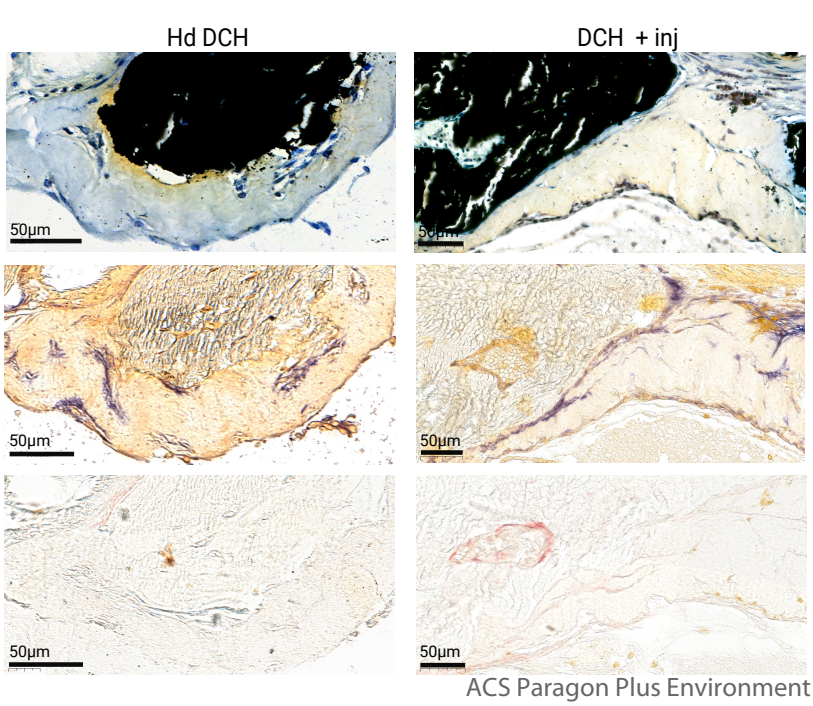
E
Hd DCH
DCH + inj
Von Kossa
ALP
TRAP
50µm
50µm
50µm
50µm
50µm
50µm

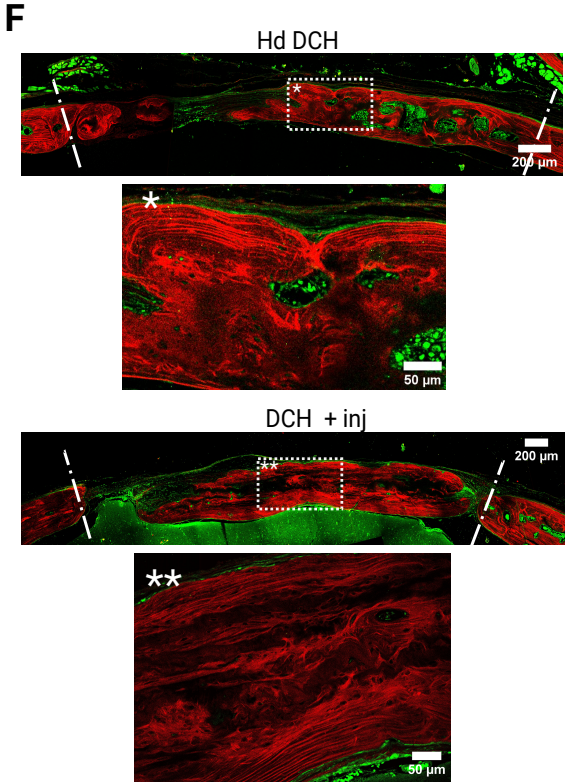
F
Hd DCH
200 µm
*
50 µm
DCH + inj
200 µm
**
50 µm